Three-Dimensional Structure Formation via Inkjet-printed Metal Nanoparticles: Ink and Application Development

Dwipayan Patnaik
Vivek Subramanian, Ed.
Sayeef Salahuddin, Ed.

Electrical Engineering and Computer Sciences
University of California at Berkeley

Technical Report No. UCB/EECS-2018-96
http://www2.eecs.berkeley.edu/Pubs/TechRpts/2018/EECS-2018-96.html

August 1, 2018

THREE-DIMENSIONAL STRUCTURE FORMATION VIA INKJET-PRINTED METAL NANOPARTICLES: INK AND APPLICATION DEVELOPMENT

by

Dwipayan Patnaik

A dissertation submitted in partial satisfaction of the

requirements for the degree of

Masters in Science

in

Engineering – Electrical Engineering and Computer Sciences

in the

Graduate Division

of the

University of California, Berkeley

Committee in charge:

Professor Vivek Subramanian, Chair

_____

Professor Sayeef Salahuddin

_____

Fall 2018

Dedicated to my mother and sister

Abstract

THREE-DIMENSIONAL STRUCTURE FORMATION VIA INKJET-PRINTED METAL NANOPARTICLES:
INK AND APPLICATION DEVELOPMENT

by

Dwipayan Patnaik

Masters of Science in Engineering – Electrical Engineering and Computer Sciences

University of California, Berkeley

Professor Vivek Subramanian, Chair

The field of printed electronics is a rapidly-emerging area of research and development primarily concerned with low-cost fabrication materials and processes for electronic devices. As conventional silicon-based electronic devices continue to push the physical boundaries of scaling to achieve increased performance for electronic devices, the field of printed electronics instead has focused on niche applications where form, function and cost are more important. However, certain applications in the realm of printed electronics are still poised for adoption to industrial processes, namely the application of printed conductors for electrical interconnects.

This work emphasizes this point by exploring different metal systems that can be used to replace eutectic solders in the modern packaging of electronic devices. The first chapter begins with a discussion of the current packaging process and provides a motivation for the need to replace solder with metallic copper in those systems. The chapter ends with an introduction to the different printing processes used throughout this work and their advantage in achieving high performance electrical interconnects. The next three chapters explore different copper systems that could potentially be used as replacement for solder in modern packages. Each of those chapters explain the synthesis process and then later delve into the details of the ink formulation process for the printed technology used. Finally, they end with an electrical and mechanical characterization of the printed features.

The last chapter in this thesis deals with the understanding of the nature of nanoparticle growth upon sintering. The chapter begins with a discussion of the different growth mechanisms involved in nanoparticle systems and their consequences on the overall morphology of the sintered films. It then relates these changes to the differences in the mechanical strengths observed in these films. Finally, the chapter ends with an explanation for these morphological differences and provides a route for using sintering profile as a control knob to tune the mechanical properties of nanoparticle systems.

Acknowledgements

During my two years in UC Berkeley, I have had a wonderful opportunity to explore myself and my interests. This would not have been possible without the continued support of my adviser, Prof. Vivek Subramanian. I would like to thank him for giving me the freedom to pursue research topics that were interesting to me and for providing me access to all the facilities in and around Berkeley. His guidance allowed me to organize my thoughts and systematically approach problems which has led to the work that you will read about in this thesis. I also must thank him for sharing his 20-year old scotch with me which was such a treat.

Next, I would like to acknowledge my parents and sister for their continued belief in me. Although sometimes they did not understand the purpose of my work here, they always encouraged me to follow my passion. Thank you Mohamed Eklaque (my brother-in-law) for taking care of things back home when I was here. I would like to especially mention my little nephew, Arhaan, here who has been the shining light in my life. I look forward to spending more time with you when I return and sharing all my wonderful experiences from Berkeley with you as you grow up. My sincerest appreciation and gratitude goes to all the other family members (especially Swetapadma Mohanty, Manjushree Mohanty, Amritraj Khattoi and Surajit Mohanty) who have made my time in graduate school so memorable.

I would like to now thank our collaborators, Texas Instruments, for continuously engaging us with intriguing research questions. Their interest in understanding the system allowed us to dig deeper into the subject. This work also could not have been completed without the assistance of our friends and staff scientists at Stanford University and the BNC facility in Stanley Hall.

Finally, the memories that I will cherish the most from my time in Berkeley, are my interactions with people who I will have the privilege of calling my closest friends for the rest of my life. Steve Volkman, thank you for instilling the confidence in me that I could be a good graduate student and for all the interesting conversations we have had over time. I have always loved having your children over at my place. Jason Hsu, for being the best lunch/golf buddy I have ever had. I have enjoyed all our time together. Andre Zeumault, for introducing me to the best food places in Berkeley. Last but not the least, my undergraduate friends (Grant Leinberger, Javan Samp, David Tomecek, Aubra Hickerson, Mellisa Raney, Katie Mass, Katheline Ferrero and Micheal Petri) for just being there for me every step of the way. I could not have done it with any one of you.

Table of Contents

Chapter 1. Introduction

The integrated circuits used in electronic devices have become increasingly complex over time. The seemingly unabated performance enhancement in these devices have been primarily achieved by continuously shrinking the individual transistors which comprise one billion or more transistors in a modern microprocessor. As a result, the electrical interconnects between the various transistors and the external components have rapidly assumed larger roles in determining the system performance. In this chapter, the modern semiconductor packaging process is discussed followed by a brief discussion of the various printing technologies. The chapter concludes by providing a motivation to explore alternative material systems to replace eutectic solder with metallic interconnects.

1.1. Semiconductor Packaging

Semiconductor packaging is a term used to describe both the structures and the processes involved in establishing a robust mechanical and electrical connection between the integrated circuits and the discrete components to form a larger system. [1] Figure 1.1 shows the relationship between the integrated circuits, interconnects and the multi-component system. Interconnects enable communication with the external world. As microprocessors and integrated circuits have continued to shrink, the packaging of these circuits has become increasingly complex and the performance of modern packages have assumed an increasingly larger role in the system performance. [2]

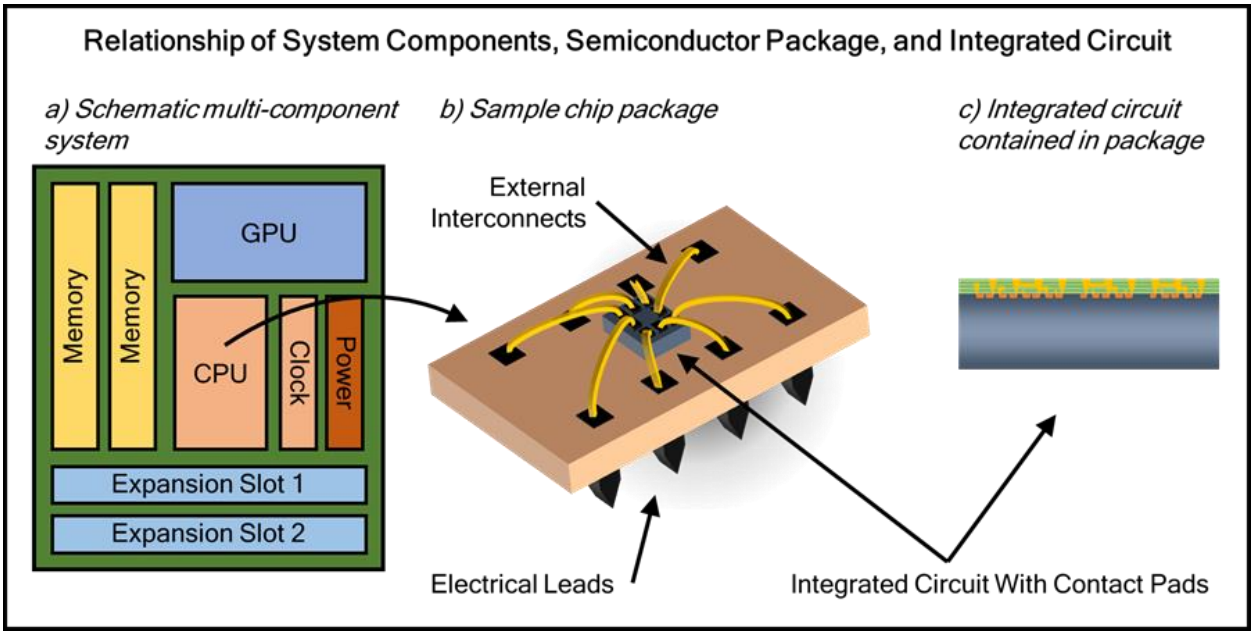

Fig 1.1: Relationship between a) a multi-component electronic system, b) a single package, and c) the integrated circuit contained in a package.

1.1.1. Semiconductor Packaging Process

The two techniques that are predominantly used in electronic packaging are wire bonding and, more recently, flip-chip bonding. The techniques are illustrated in figure 1.2. As shown in Fig 1.2 (a), wire bonding involves making a connection between the integrated circuit bond pad and the package bond pads by feeding a wire through a custom tool that automatically bonds and breaks the wire. The materials used for wire bonding typically tend to be highly conductive metals such as gold and copper. Although this technique can provide good electrical and mechanical contact between the components, one of its biggest drawbacks are that the connections are restricted to the periphery of the package. As a result, attempts to use the center of the contact pad for connection may result in shorts along the edge of the chip. Moreover, this method requires a larger footprint on the chip making it undesirable for scaled circuits.

The other technique that has become the standard in modern devices is flip-chip bonding. As illustrated in Fig 1.2 (b), in the flip-chip bonding process, the chip is oriented such that

the integrated circuit contact pads are facing downwards. This allows for a direct contact between the integrated circuit and the package, thus reducing the lateral area covered by each bonded chip. Furthermore, this technique also allows for interconnects to be placed throughout the contact pad without running the risk of shorting. The common materials used for flip-chip bonding today are lead-tin eutectic solder. Figure 1.2 outlines the bonding process for eutectic solder bumps used in flip-chip bonding.

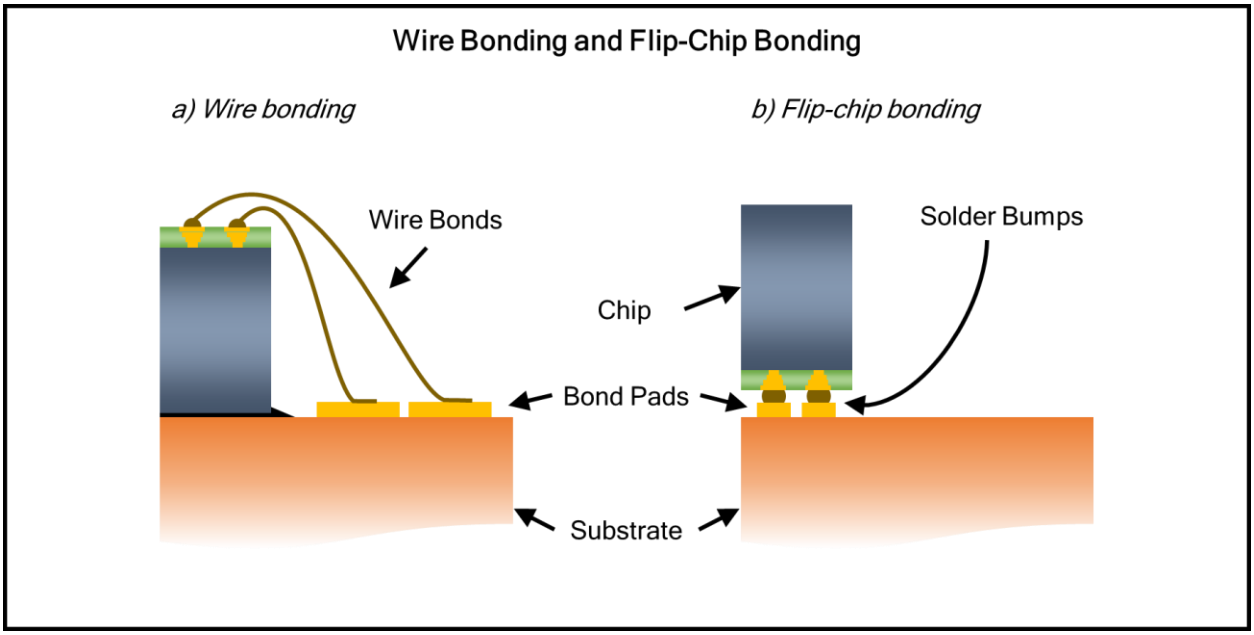

Fig 1.2: The two electronic packing techniques: (a) Wire bonding and (b) Flip-chip bonding.

As shown in Fig 1.3, the solder paste is first placed onto each bond pad on the chip as well as on the package. Then, the chip is heated using a carefully controlled heat treatment to the solder's eutectic temperature. For lead-tin solder, this temperature is close to 180 ^{0}C. At this temperature, the eutectic material changes from a solid to a liquid phase. Due to differential wetting between the bond pad and the passivation layer on the chip, the solder forms a ball. This process is known as reflow. Then, using a special tool (usually a flip-chip bonder), the chip is picked up and placed upside down on the bond pad of the package substrate. A final reflow process is conducted resulting in a robust electrical and mechanical connection between the two pads.

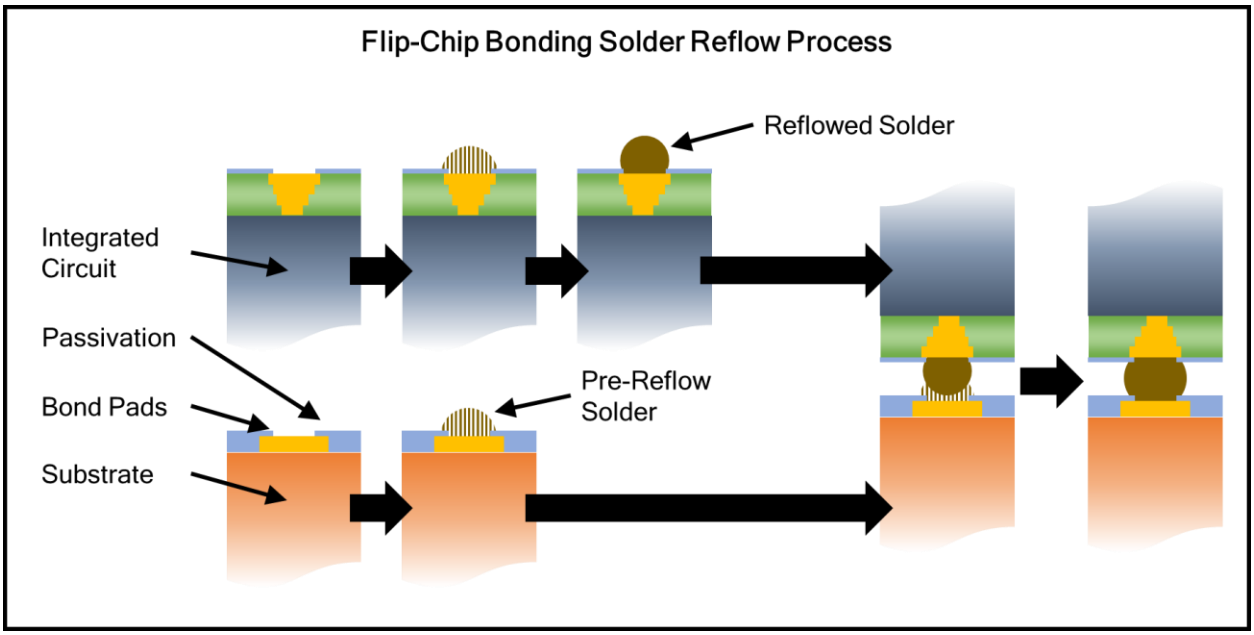

Fig 1.3: Eutectic solder reflow process and Flip-chip bonding.

1.1.2. Performance Metrics for Interconnects

As discussed earlier, the fundamental functionality of electrical interconnects is to provide both robust electrical and mechanical connection between the integrated circuit and the external components. As a result, material properties like conductivity, elasticity and shear strength are three critical performance metrics. Increased conductivity reduces power loss, making the overall system more efficient. Moreover, since the packages are subjected to both normal and transverse forces during use, both the elastic modulus and the shear strength of interconnects must be sufficient to prevent mechanical failures. The current state-of-the-art lead-free solders have resistivity around 7.7 μΩ-cm while their elastic modulus and shear strengths are 15.7 GPa and 210.09 kg/cm^2. [3] Generally, wire bonding results in better electrical performance than flip-chip bonding due to higher conductivity of materials used. While on the other hand, flip-chip bonding results in higher mechanical strengths due to the robustness of the reflowed solder balls compared to the fragile wire bonds. However, both processes encapsulate their bonds with a filler material to improve the mechanical performance of the package.

1.1.3. Packaging Form Factors and Subtractive Deposition Techniques

Packages have thus far successfully evolved to meet continuously-evolving performance and size demands. The clearest way to observe this evolution is to compare the count of the electrical leads in packages as a function of integrated circuit transistor count. Figure 1.4. shows the exponential growth of integrated circuit transistor count as a function of time (often referred to as Moore's Law [4]). Moreover, Table 1.1. also presents a comparison between the line-width requirements for each of the packaging form factors. As can be inferred from the figures below, as the density of transistors have increased on the chip, the line and widths of the interconnects have continued to shrink to maintain the performance advantages.

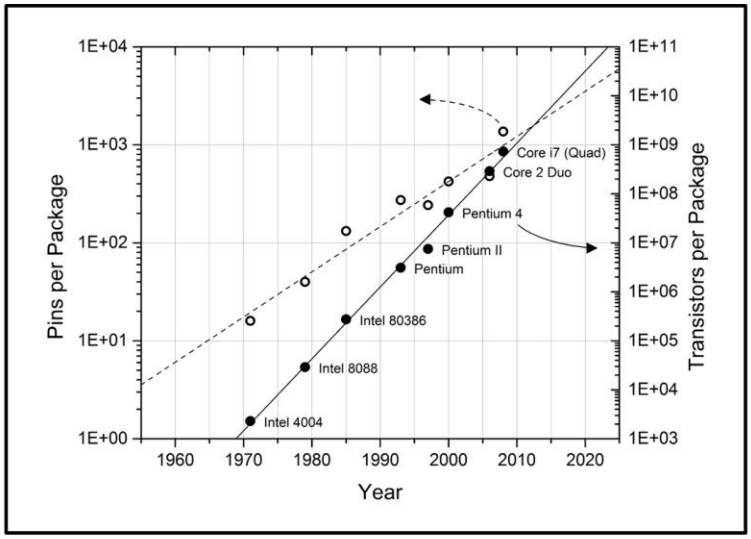

Processor	Package
4004	DIP
8088	DIP
80386	PGA
Pentium	PPGA
Pentium II	Slot
Pentium 4	PGA-ZIF
Core 2 Duo	BGA
Core i7 (Quad)	LGA

Fig 1.4: IC scaling trends as a function of transistor count and pins per package. Insert table identifies package form factor for respective packages.

		DIP	QFP	PGA	BGA	LGA
Leads	Type	Leadframe	Gull Wing	Pin	Solder Ball	Pad
	Arrangement	Row	Row	Array	Array	Array
	Count	4 – 64	32 – 304	169 – 940	196 – 615	771 – 2011
	Width [µm]	380 – 500	220 – 450	200 – 500	400 – 600	250 – 630
	Pitch [mm]	1.78 – 2.54	0.40 – 1.00	1.27 – 2.54	1.00 – 1.27	0.50 – 1.27
Mount	Through-Hole	Y	--	Y	--	--
	Surface Mount	--	Y	--	Y	Y
	Socket	Y	--	Y	--	Y
Interconnects	Wire Bond	Y	Y	Y	Y	Y
	Materials	Copper, Gold, Silver Alloys				
	Width [µm]	12.5 – 75				
	Pitch [µm]	35 – 60				
	Flip Chip	--	--	Y	Y	Y
	Materials	--	--	Solder Alloys, Copper Pillars, Gold Stud Bumps		
	Width [µm]	--	--	20 – 50		
	Pitch [µm]	--	--	40 – 250		

Table 1.1: Lead, Mount and interconnect details for commonly used electronic packages.

Although a significant amount of investment has undeniably driven integrated circuits performance up and costs down, there are still several issues that need to be addressed. One of the primary constraints is that all material and process related advances have been required to be compatible with silicon substrates. This has resulted in the development of a series of subtractive process cycles (material deposition followed by lithography followed by etching) which factor strongly in the overall cost of the final product. While these subtractive processes are generally still necessary for producing complex, sub-micron features, they may no longer be necessary for feature sizes greater

than ten microns leading to cost minimization as much as possible. As a result, the following section will discuss an additive manufacturing technique that can be used as an alternative to the afore mentioned subtractive techniques.

1.2. Printing Technologies

As mentioned previously, the semiconductor industry has advanced in an incredibly fast pace since the 1960s driven primarily by improvement in device performance by scaling. Therefore, several subtractive methods have been developed to keep the processes compatible with silicon. However, these processes significantly add to the cost of manufacturing making it necessary to seek alternative deposition/patterning techniques. In this section, two deposition techniques have been discussed that might be useful for feature sizes larger than 10 microns.

1.2.1. Inkjet Printing

Inkjet printing is an additive process which is capable of producing features on the order of tens of microns. Since it is an additive process, it can be used to deposit materials only where they are required. This can potentially offer cost savings due to the minimization of materials utilized and the minimization of process steps used for fabrication. Although inkjet printing has been traditionally employed for deposition of inks on paper, new development in inkjet printing capabilities have made it possible to print functional electronic inks on a variety of substrates (like plastic).

Figure 1.5 shows the various components of an inkjet printing system. The printhead/nozzle used to eject inks is the heart of the system. An ink supply is attached to the printhead and a pressure control system both forces the ink to the printhead and controls the shape of the ink meniscus at the nozzle orifice. A jetting control system, also attached to the printhead, is used to generate and deliver electronic pulses to the nozzle which facilitate drop ejection. The motion control system allows movement of the printhead and stage along three degrees of freedom: two translational (X and Y) and one rotational. Most printers include a vision control system which aid in substrate alignment and mid-flight drop observation to guarantee reliable jetting. Finally, a temperature control system is used to control the temperature of both the stage and the nozzle as per the process requirements. Most control systems are typically controlled by a computer which provides the necessary input signals to the various components.

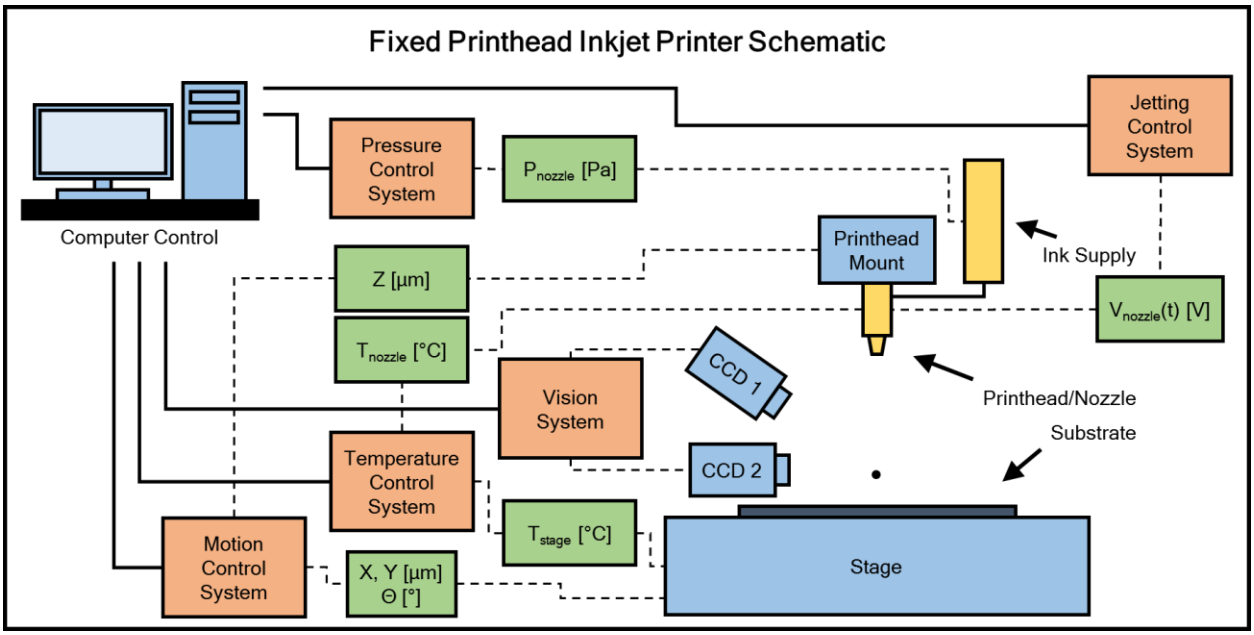

Fig 1.5: Schematic showing the layout of a typical inkjet printer. The blue blocks represent physical hardware while the orange and green blocks represent the various control systems.

There are several mechanisms for drop formation in inkjet printing, namely thermal and piezoelectric. [5] The method used for this work was based on a piezoelectric print head. In this system, piezoelectric nozzles are built with a film of piezoelectric material positioned along the wall of the chamber. When a voltage signal is applied on the piezoelectric material, it deflects inwards to push a small amount of ink out of the nozzle. When the signal returns off, the material relaxes and the chamber refills. This process is repeated multiple times to generate ink droplets. Figure 1.6 (a) describes the mechanism of a piezoelectric printhead. Another classification used to differentiate inkjet printers are based on their jetting frequency. The two classes of techniques are called continuous and drop-on demand. [5] The inkjet printer used for our study used the drop-on demand technique. A DOD (Drop-on Demand) inkjet printer ejects a discrete droplet from the nozzle whenever the nozzle is actuated, unlike a continuous stream of fluid that is expelled in the case of a continuous jetting printer. This signal is provided by the jetting waveform which is used to deflect the piezoelectric material present in the printhead. This allows ejection of ink droplets at a specified frequency. Figure 1.6 (b) illustrates a DOD (Drop-on Demand) inkjet printer.

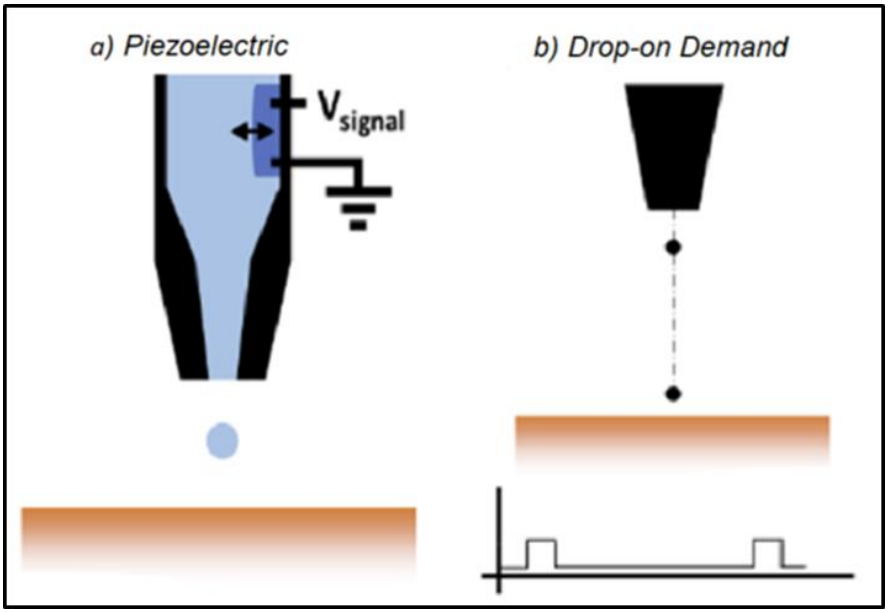

Fig 1.6: Schematic showing (a) a piezoelectric printhead used for droplet formation and (b) a Drop-on Demand inkjet printer.

One of the major components of inkjet printing is the formulation of an ink suitable for ejection through a nozzle. Figure 1.6 shows the relevant jettability window for inks in the Capillary number (Ca) and Weber number (We) parameter space which is used as a metric to determine printability of various inks. [6] The definitions of these parameters are provided below. Inks that fall within the window are considered suitable for inkjet printing. However, the ones that remain outside can be tuned by using different solvent system or by altering their mass loading in order to push them back into the jettability window. This metric has been used throughout this work to determine the jettability of inks.

$$\text{Capillary number (Ca)} = \frac{\text{viscous force}}{\text{surface tension}} = \frac{\eta v d}{\sigma d} = \frac{\eta v}{\sigma} \qquad (1)$$

$$\text{Weber number (We)} = \frac{\text{inertial force}}{\text{surface tension}} = \frac{\rho v^2 d^2}{\sigma d} = \frac{\rho v^2 d}{\sigma} \qquad (2)$$

where η, ρ and σ are the viscosity, density and surface tension of the ink and v and d are the droplet velocity and the nozzle diameter respectively.

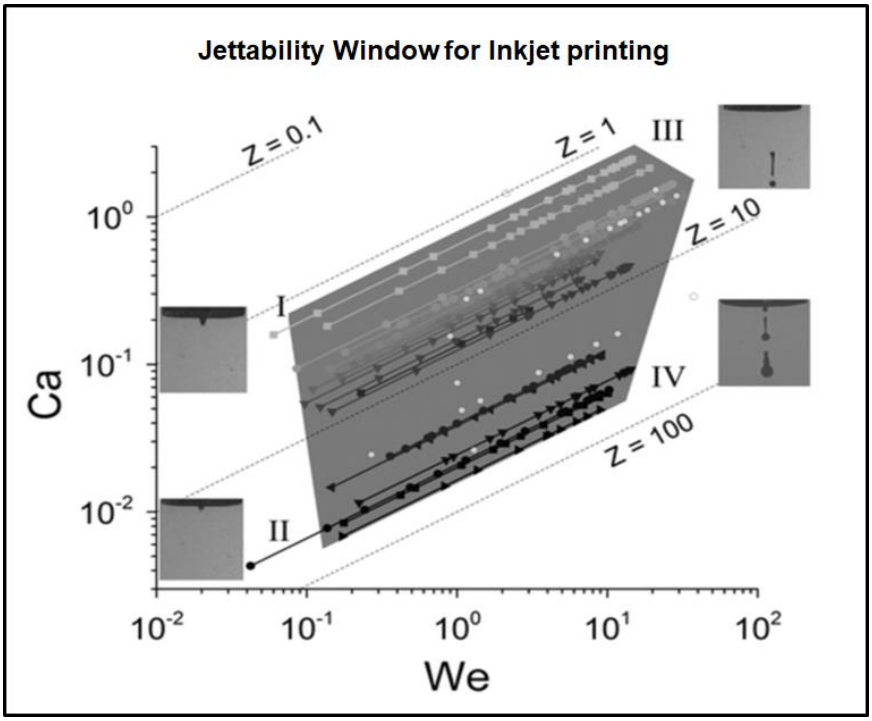

Fig 1.7: Jettability window for inkjet printing in the capillary number-Weber number parameter space.

The standard waveform used to print most inks is a bipolar waveform (shown in Figure 1.8). In this waveform, the voltage is ramped from an initial voltage (V_0) to a final voltage (V_1) within a defined time (t_{rise}). During this time the piezoelectric head on the nozzle expands to expel some of the ink out of the nozzle. After that, the waveform is allowed to sit at V_0 for a time (t_{dwell}) during which the actual drop ejection occurs. Following that, the voltage is dropped to the final voltage of the negative pulse (V_2) within a time (t_{fall}) where it is sustained for a time (t_{echo}). This section of the waveform serves to eliminate ejection of residual drops by sucking the ink back into the nozzle. Finally, the voltage goes back to its initial value (V0) within time (t_{rise}). This modulation is repeated with a certain frequency (referred to as the jetting frequency) to generate multiple drops during printing.

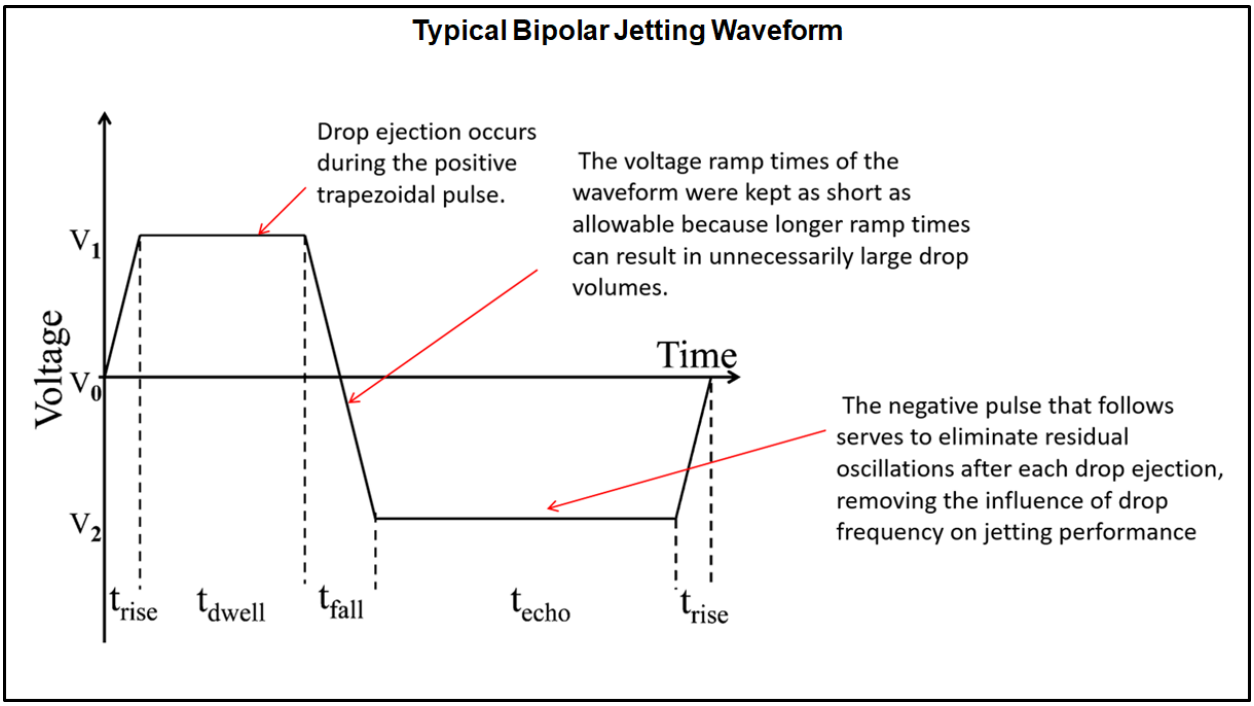

Fig 1.8: A typical bipolar jetting waveform showing the various waveform parameters (Voltage, Dwell time, Rise/Fall times) and their functions during printing.

1.2.2. Stencil Printing

Stencil printing, just like inkjet printing, is another additive process that is used to deposit materials on different substrate. Figure 1.9 shows a typical process flow for stencil printing. In this technique, a mask of the desired pattern in placed on the surface of the substrate on which the material is to be deposited. The mask is aligned with the substrate such that only the patterns on the mask get transferred onto the surface while the rest of the substrate is covered by the mask. Then, a doctor blade is used to level the ink on the mask to achieve a uniform film. The thickness of the film is determined by the thickness of the mask used. Finally, the mask is removed and the film in dried and annealed to obtain the final feature. This technique is typically used to transfer solder paste onto lead frames before the solder reflow process that was discussed earlier. The inks used for stencil printing usually have higher viscosities than the inks used for inkjet printing.

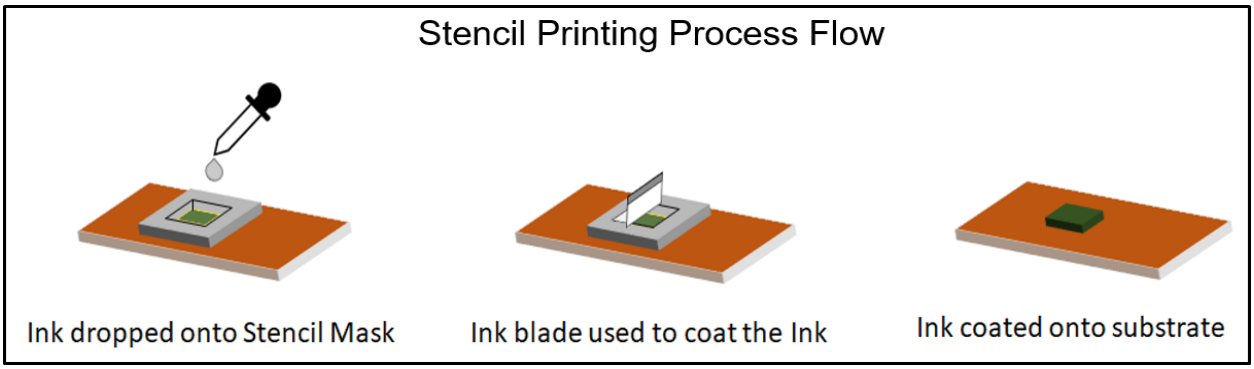

Fig 1.9: Schematic showing the typical process flow for stencil printing.

1.3. Electronic Inks for Metallic Interconnects

Although eutectic solders are predominantly used for electrical interconnects, they suffer from low conductivity and worse electromigration performance. Therefore, new materials and processes must be explored that can overcome these limitations while still maintaining process temperatures that do not exceed current thermal budgets. In this section, two interesting materials are introduced, namely metal nanoparticles and metal solution-gels, which can potentially satisfy all the above conditions. More importantly, these materials can also be used to formulate inks to deposit materials using the printing technologies discussed above.

1.3.1. Metal Nanoparticle Inks

Despite the wide variety of materials and inks used in printed electronics applications, perhaps the most commonly used type of inks are inorganic metal nanoparticle inks. These are widely used because they provide a pathway to achieve conductive interconnects without exceeding the current process temperatures. In a metal nanoparticle ink, the metal nanoparticles are typically synthesized using liquid-phase colloidal synthesis techniques. [7] The particles are encapsulated by carbon-based materials which bind to the nanoparticle core. These encapsulants prevent the functional solids from interacting with each other, thereby preventing potential aggregation within the ink. Finally, these particles are dispersed in some solvent which functions to stabilize the solid material in order to carry it to the substrate.

As mentioned above, the reason metal nanoparticles are preferred over organic alternatives is due to their ability to achieve highly conductive films at processing temperatures below 200 ^{0}C. This is achieved by taking advantage of a phenomenon called melting point depression, whereby nanoscale materials exhibit dramatically lower melting temperature than their bulk counterparts. [8] Figure 1.10 shows the melting point depression curve for gold. This depression of melting point is due to the increase in the surface area-to-volume ratio of the nanoparticles which strains the bonds between their atoms. This results in a decrease in energy required to initiate melting, thus lowering the melting point of the overall system.

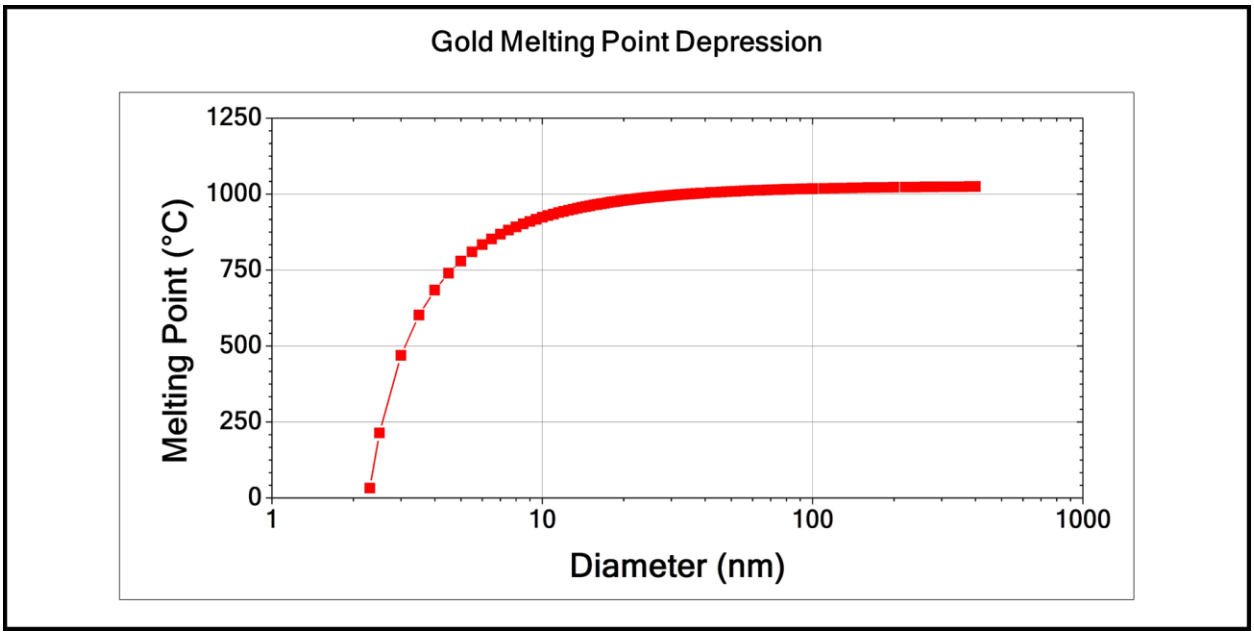

Fig 1.10: Curve showing the melting point depression of gold particles.

After the metal nanoparticles have been deposited and dried, they do not immediately exhibit high conductivity. This is due to the encapsulants that are still bound to the nanoparticles. Thus, thermal treatments are often used to de-encapsulate the particles so that they can interact with each other to form a continuous film. Figure 1.11 shows the schematic for the sintering process. As heat is provided to the system, the bond between the encapsulant and nanoparticle breaks and the encapsulants act as secondary solvents to initiate coalescence of the particles. Upon coalescing, the particles diffuse into each other to form larger particles and ultimately a continuous film. [9] However, there are different pathways for particle growth which lead to different morphologies of the sintered film. These have been discussed in Chapter 5.

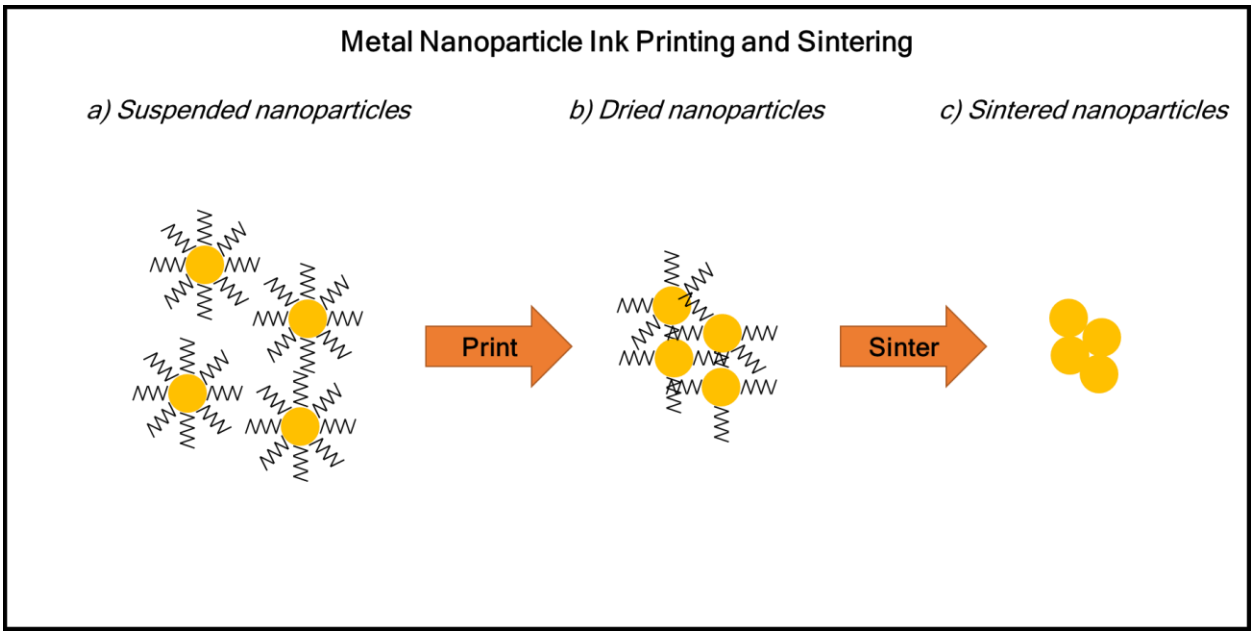

Fig 1.11: Schematic representation of the metal nanoparticle sintering process. a) Suspended nanoparticle inks are printed, b) dried nanoparticles still contain encapsulants that prevent conductive films, c) sintered nanoparticles containing little or no encapsulants form continuous film.

1.3.2. Metal Solution Gel Inks

The other material system that can help provide conductive films at low temperatures is the metal solutions-gels, commonly referred to as metal sol-gels. These inks typically consist of metal salts that are present in a solvent system with some reducing agent. Figure shows the schematic for a metal oxide sol-gel conversion process. The entire conversion process involves two steps: a low temperature drying step and a high temperature annealing step. In the low temperature step, the wet sol-gel film is dried as the solvents are removed. This typically begins as soon as the material is deposited on the substrate. Following that is a high temperature step which facilitates the reduction of the metal salts into pure metal. In this step, the particles undergo densification to finally form a continuous film. [10]

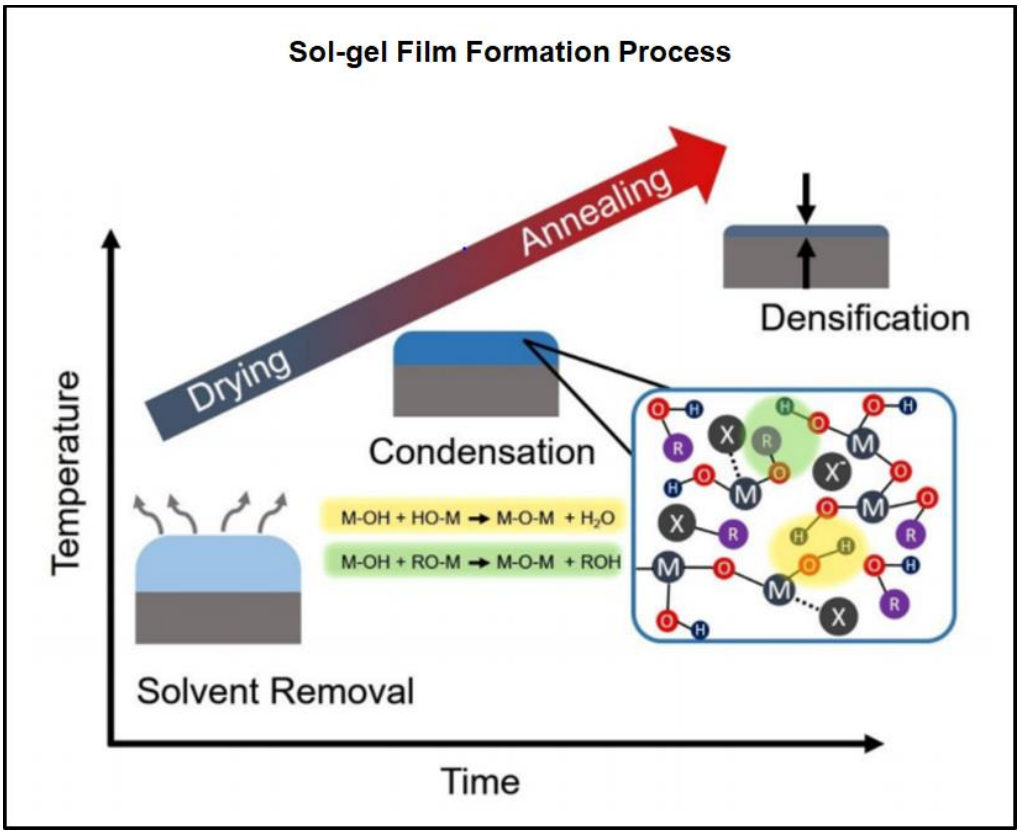

Fig 1.11: Sol-gel film formation process showing film drying, condensation and film densification.

1.4. Thesis Outline

While the primary interests in printed conductors have been planar applications to date, the material and process development for three-dimensional interconnects may prove to be a viable alternative to conventional packaging materials and processes. From ink design to process development and characterization, all aspects of this application will be explored in this dissertation, which will be organized in the following manner:

Chapter Two will explore the use of a commercial copper ink as a potential replacement for eutectic solder in electronic packaging applications. The processing technique used for the deposition of the ink will be discussed followed by an electrical and mechanical characterization of the resulting films.

Chapter Three will visit the use of copper sol-gels for the same application. The chapter will begin with a discussion of sol-gel formulation process and the resulting inks that can be designed for inkjet printing. Thereafter, the chapter will end with brief note on the mechanical and electrical properties of the converted films.

Chapter Four will discuss the formulation of an in-house copper nanoparticle system. It will cover the nanoparticle synthesis technique and the ink formulation ideas for both inkjet and stencil printing. This chapter will, again. conclude with a discussion of the electrical and mechanical properties of the sintered nanoparticle films.

Finally, Chapter Five discusses the importance of processing parameters on the overall properties of the sintered films. In particular, the chapter will discuss how the change in temperature ramp rate during sintering can influence the mechanical strength of the films. It will end with an explanation for the evolution of films during the sintering process.

Chapter 2. Commercial Nanoparticle Inks (Pvnanocell)

The first attempt to use metallic copper for electronic packaging application was through a commercial copper nanoparticle ink supplied by Pvnanocell (Sicrys^{TM} IC50TM-8). This ink was based on single-crystal copper nanoparticles mixed in triethylene glycol monomethyl ether (TGME) as the solvent. The following sections provide details on the printing process and the electrical and mechanical characterization of the commercial ink.

2.1. Inkjet Printing of Commercial Ink

As discussed in Chapter 1, the ink's fluid properties and jetting waveform are the keys controls used to enable jetting through an inkjet printer. These metrics for the commercial ink have been presented in this section. Finally, this chapter ends with a discussion about the use of hydrophobic solvents as passivation layer on the nozzle in order to change the wetting properties of the print head to enhance printability of the commercial ink.

2.1.1. Ink Properties and Jetting Waveform for Commercial Ink

The properties of the commercial ink are listed in Table 2.1. [11] These values were provided by the supplier and were further verified after the procurement of the ink from the vendor. More importantly, these fluid properties allowed the commercial ink to fall within the jettability window which is a prerequisite for inkjet printing (as discussed in Chapter 1).

Properties	Typical Values
Mass Loading	50 %
Viscosity	32 cP
Surface Tension	34 mN/m
Specific Gravity	1.85 g/mL

Table 2.1: Fluid properties of the commercial nanoparticle Ink (Pvnanocell).

The jetting waveform used to print the commercial ink is shown in Figure 2.1. The waveform parameters (like Voltage, Dwell time, Rise/Fall times etc.) were provided by the supplier and thus an extended jetting experiment was not conducted to determine those parameters for the ink. The purpose and influence of each section of the jetting waveform was previously discussed in Chapter 1.

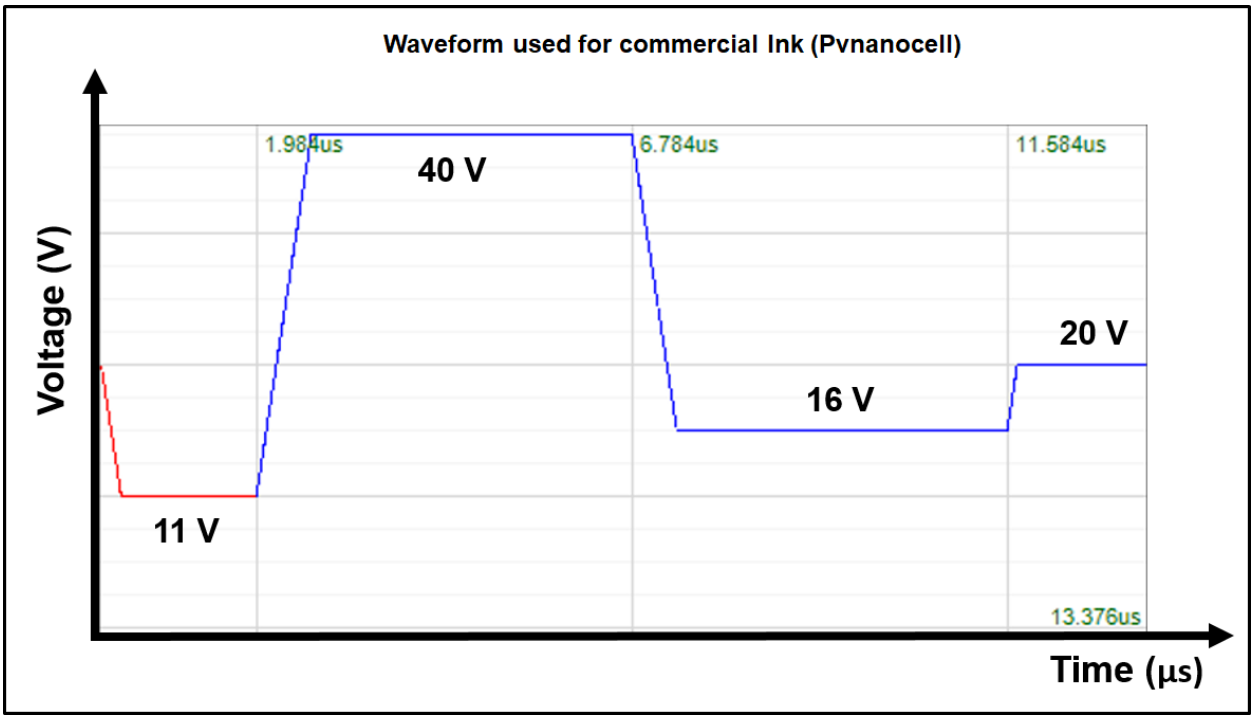

Fig 2.1: Jetting Waveform for the commercial nanoparticle Ink (Pvnanocell).

2.1.2. Nozzle Head Treatment for Reliable Jetting

One issue that was encountered during the initial screening studies of the commercial ink was the inconsistency in the printed lines due to the formation of satellite drops as shown in Fig. 2.2 (a). Satellite drops in the context of printing are defined as unwanted small droplets that fall away from the originally intended target. [12] These inconsistencies were determined to be due to the interaction of the ink with the printhead.

The printheads in the cartridges used for inkjet printing (Fujifilm Dimatix 10pL cartridge) were based on silicon MEMs (Microelectromechanical systems) which are hydrophilic in nature. Moreover, TGME, the solvent used in the commercial ink, is also a known hydrophilic solvent. Therefore, during printing whenever the ink encountered the printhead, it would wet its surface instead of being completely ejected out of the nozzle. Thus, over time this accumulation of ink around the surface of the nozzle led to inconsistent drop ejection and satellite drop formation.

In order to remedy the problem, a hydrophobic treatment of the printhead was performed to minimize the interaction of the ink with its surface. In this treatment, a solution of 10 mL Trichloro(octadecyl) silane diluted with 20 mL of Toluene was used to coat the surface of the printheads. The chlorine groups present in the silane interact with the silicon while the rest of the carbon groups hang as dangling bonds off the surface. This orientation of Trichloro(octadecyl)silane prevents the interaction of TGME with the silicon surface making it hydrophobic in nature. [13] As a result, the wetting of the ink on the nozzle surface was significantly decreased leading to consistent drop ejection and smoother printed lines as shown in Fig. 2.2 (b).

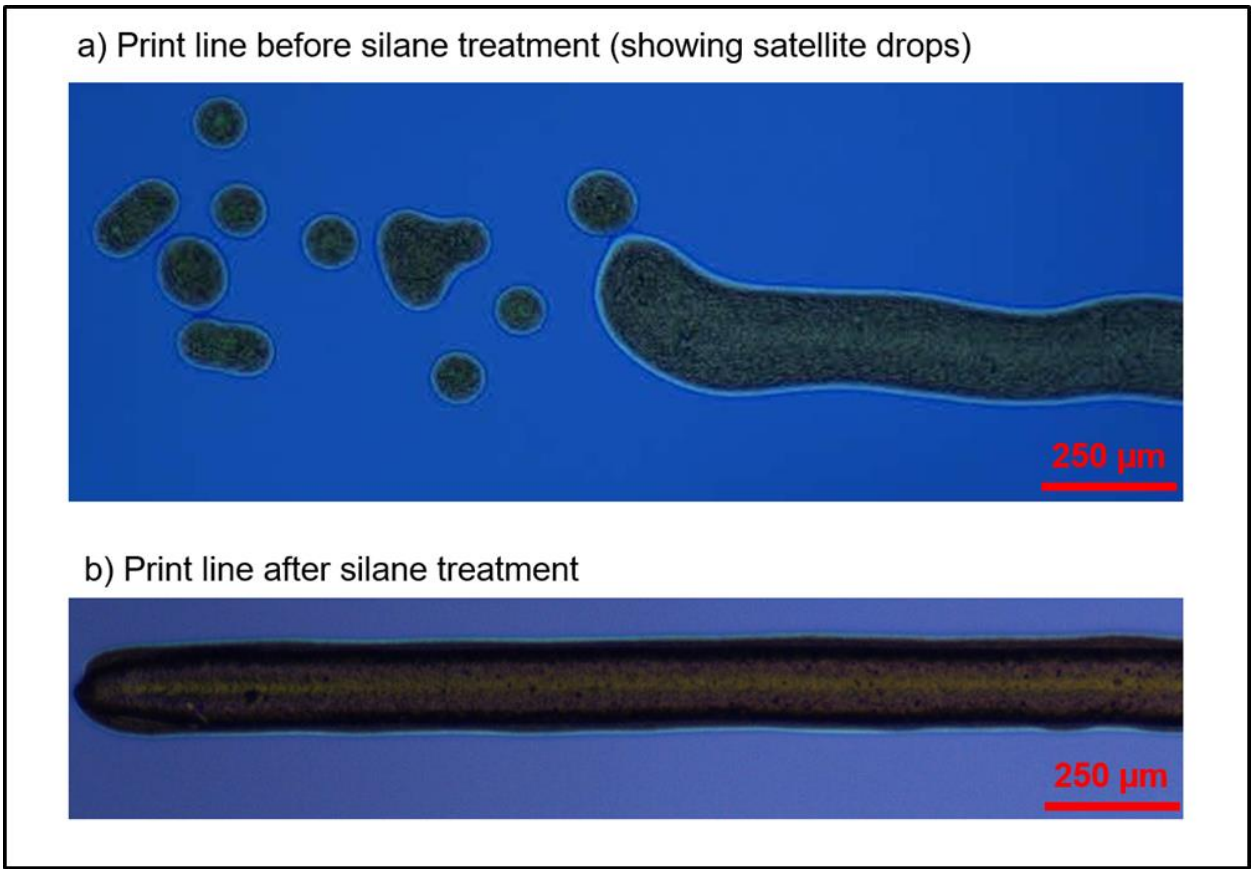

Fig 2.2: (a) Print line before silane treatment (showing satellite drops), (b) Print line after silane treatment.

2.2. Electrical Characterization of Pvnanocell Ink

The graph below (Fig 2.3) shows the electrical resistivity of the commercial ink as a function of the sinter temperature and environment. The red line in the graph indicates the resistivity value that is ten times the bulk resistivity of copper (1.72×10^{-5} Ω-cm). This was used as a benchmark to imply the onset of conductivity of the printed copper films.

As shown in the figure, sintering in air did not provide conductive films due to the partial oxidation of the copper nanoparticles prior to sintering. An EDS (Energy Dispersive X-ray Spectroscopy) analysis of the films showed an oxygen content of more than 40 % in the films. This is discussed in the sit time study analysis that is presented following this discussion. Sintering in nitrogen and forming gas environments, on the other hand, provided conductive films at temperatures above 300 ^{0}C. The presence of hydrogen in forming gas (H_2+ N_2) acts as a reducing agent to dissociate the long-chained carbon ligands that surround the nanoparticles, thus enabling sintering in these systems. This was confirmed by an elemental analysis of the films using which showed a higher percentage of carbon present in the films sintered in nitrogen (18 %) compared to forming gas (10%). This provides a direct explanation for the difference in the resistivity values between the two sintering environments.

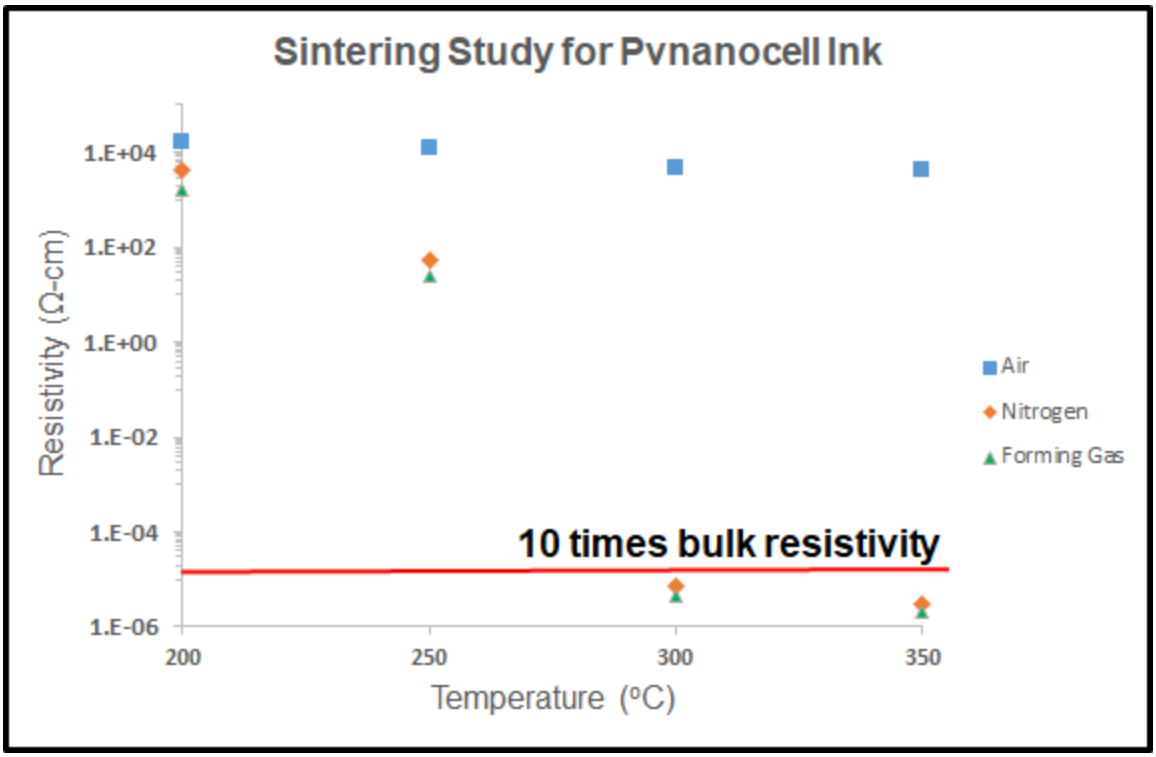

Fig 2.3: Sintering study of Pvnanocell Ink showing resistivity as a function of sinter temperature and environment. The red line indicates the resistivity value that is ten times the resistivity of bulk copper (1.72×10^{-5} Ω-cm).

Copper particles are susceptible to oxidation in the presence of air. As a result, it was important to get a sense of the stability of copper particles during the processing window. This was accomplished by conducting a sit time study to understand the degradation time of the copper particles in the commercial ink. The following graph (Fig 2.4) shows the impact that exposure in air has on the electrical properties of the commercial ink. In this experiment, the ink was exposed to ambient air for a defined amount of time and then sintered in either nitrogen or forming gas environments for 1 hour at 300 ^{0}C. As can be seen from the graph, the resistivity of the sintered films varied significantly with increased exposure time. An EDS analysis of the films determined that it was due to the partial oxidation of the copper nanoparticles upon exposure to air. Films that were exposed for more than 15 mins had an oxygen content ranging from 40 – 60 %. This metric was useful for our experiments as all the pre-sintering processes like ink transfer/loading and printing were conducted in air. As a result, this study helped in defining a cut-off of 10 mins for all the pre-sintering procedures to prevent significant degradation of the ink prior to sintering.

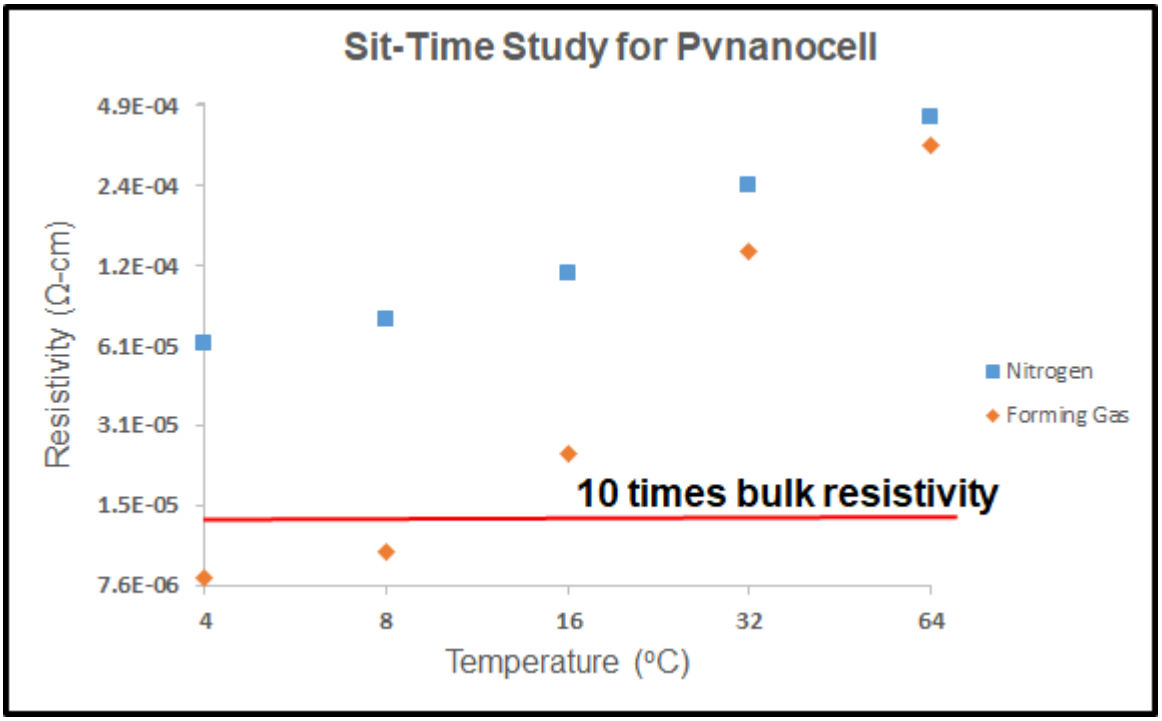

Fig 2.4: Sit time study of Pvnanocell ink showing resistivity as a function of exposure time in air (prior to sintering) and sinter environments. The red line indicates the resistivity value that is ten times the resistivity of bulk copper (1.72×10^{-5} Ω-cm).

2.3. Mechanical Characterization of Pvnanocell Ink

The mechanical characterization of the commercial ink was done by measuring the shear strength of the sintered printed lines as a function of applied force. The experimental setup for the bonding experiment is shown in Fig 2.5. In this experiment, a 500-nm film of copper was deposited onto a SiO_2 wafer using an Electron-beam evaporator. Then, an array of copper lines was printed on this surface using an inkjet printer (Fujifilm Dimatix Materials Printer DMP-2850). The length, width and height of each printed line was 1 cm, 150 µm and 1.5 µm respectively with a pitch of 0.5 mm covering a total area of 1 cm^2. Following that, a copper die was placed upside down on top of the printed surface and was flip-chip bonded (Finetech Flip Chip Bonder) under the application of a defined force. The entire bonding process was done in air. After the bonding process was completed, the bonded samples were transferred to glove box where the films were sintered under a nitrogen environment for 1 hour at 300 ^{0}C. Finally, a bond tester (Mbraun Bond Tester) was used to apply a shear force on the bonded region to study mechanical strengths/failures of the structures.

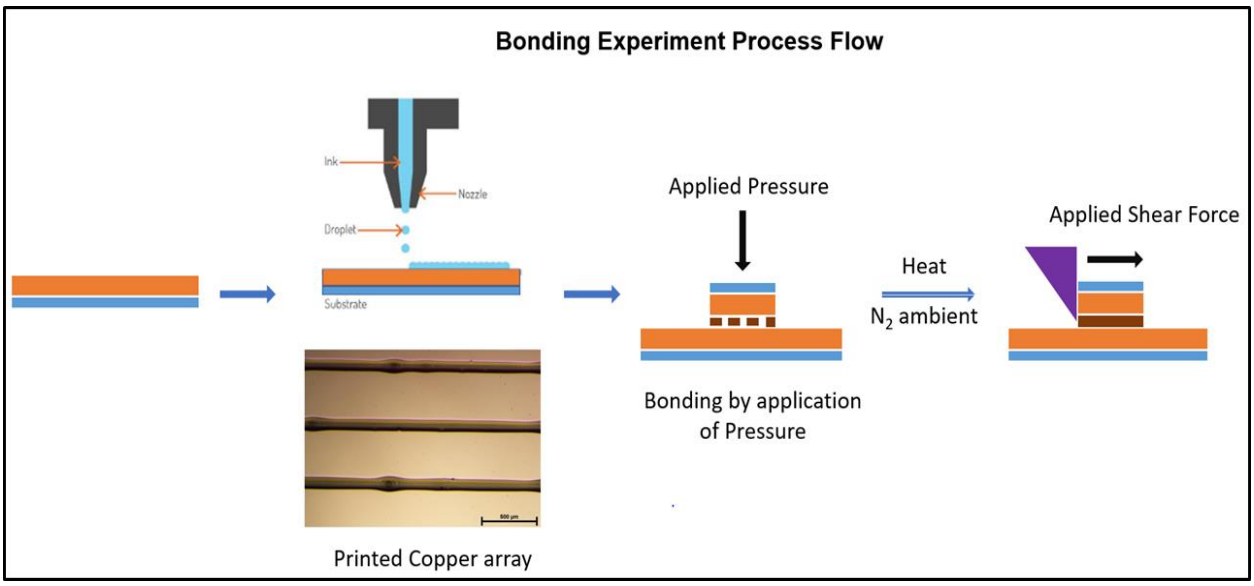

Fig 2.5: Schematic showing the experimental setup for the bonding studies.

Figure 2.6 shows the results of the bonding study. As can be seen from the graph, the shear strengths of the bonds increase with increasing applied force. This was expected due to stronger binding of the copper nanoparticles to the evaporated copper surface at higher applied force. However, no significant improvement in shear strength was observed for samples bonded for 1 hour compared to 30 seconds implying that a bonding time of 30 seconds was sufficient to impart complete contact between the two surfaces. Finally, the bond strengths demonstrated by these copper bonds were comparable to the state of the art eutectic solder systems (Shear Strength = 210.09 g/cm^2) used in industry. [14] Thus, making them a viable alternative to lead-based solder interconnects that are used in most integrated circuits today.

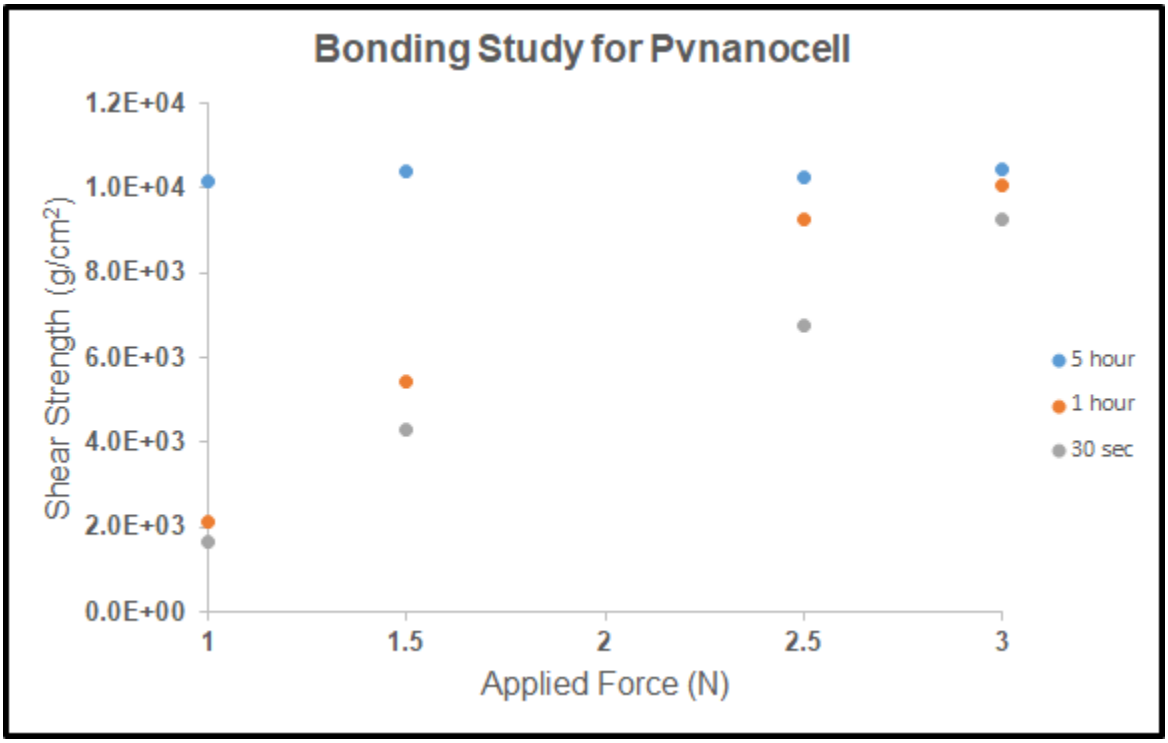

Fig 2.6: Shear Strengths of the bonded copper nanoparticles dies as a function of applied force and bonding time.

The figures below (Figure 2.7) show the bonded nanoparticle region pre- and post-failure. As can be seen from the cross-sectional images, the failure occurs within the nanoparticle region and not along the contact interface between the nanoparticle and evaporated copper. This indicates that the nanoparticles bind strongly to evaporated copper and that the weakest point along the cross section is somewhere within the nanoparticle film itself. This, as will be discussed next, is due to the partial sintering of the copper nanoparticle in the bulk of the film.

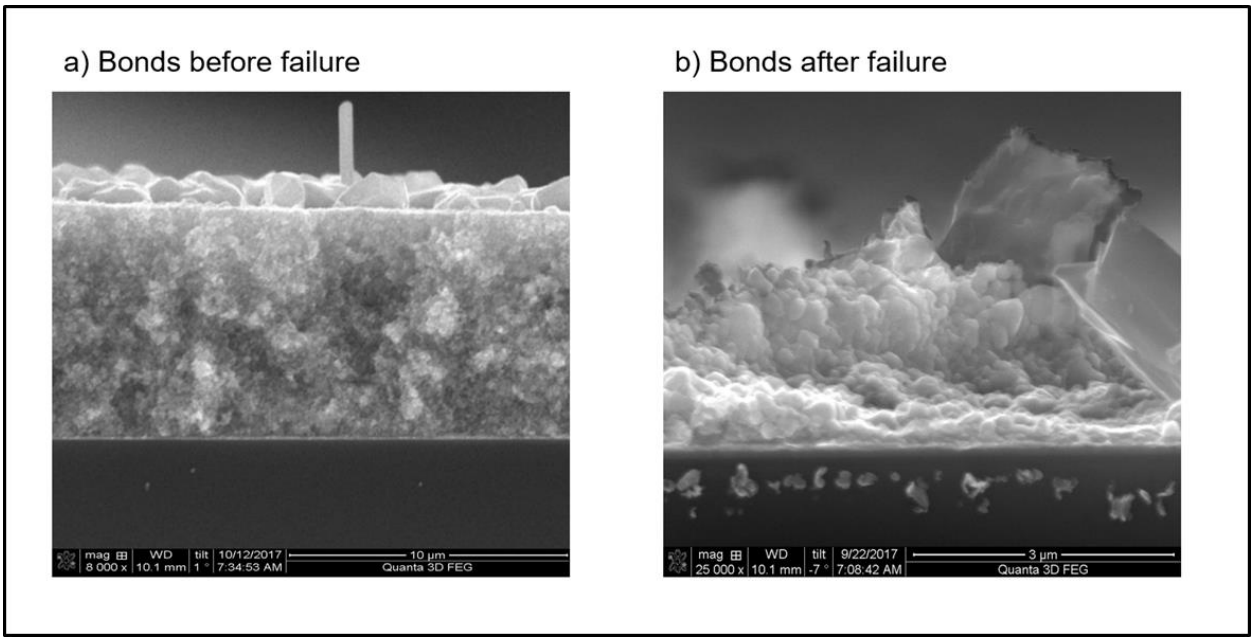

Fig 2.7: Cross-section of the nanoparticle bonding surface before and after failure showing failure within the nanoparticle film.

Figure 2.8 shows a top-down SEM (Scanning Electron Microscopy) image of the failed bonded interfaces. As shown in the figure, the failures occurred along defined domains. An EDS analysis along different region of the surface revealed the differences in the amount of carbon present in the film. For example, the lighter regions in the image contained a much higher percentage of carbon (54%) compared to the darker region (24%). This difference in the amount of carbon present indicated partial sintering which is responsible for making the film weak at those regions. There was also some residual oxygen (10 - 12%) that was found in these films which could have been due to either partial oxidation of the nanoparticles or trapping of the oxygen molecules in the film during the bonding process.

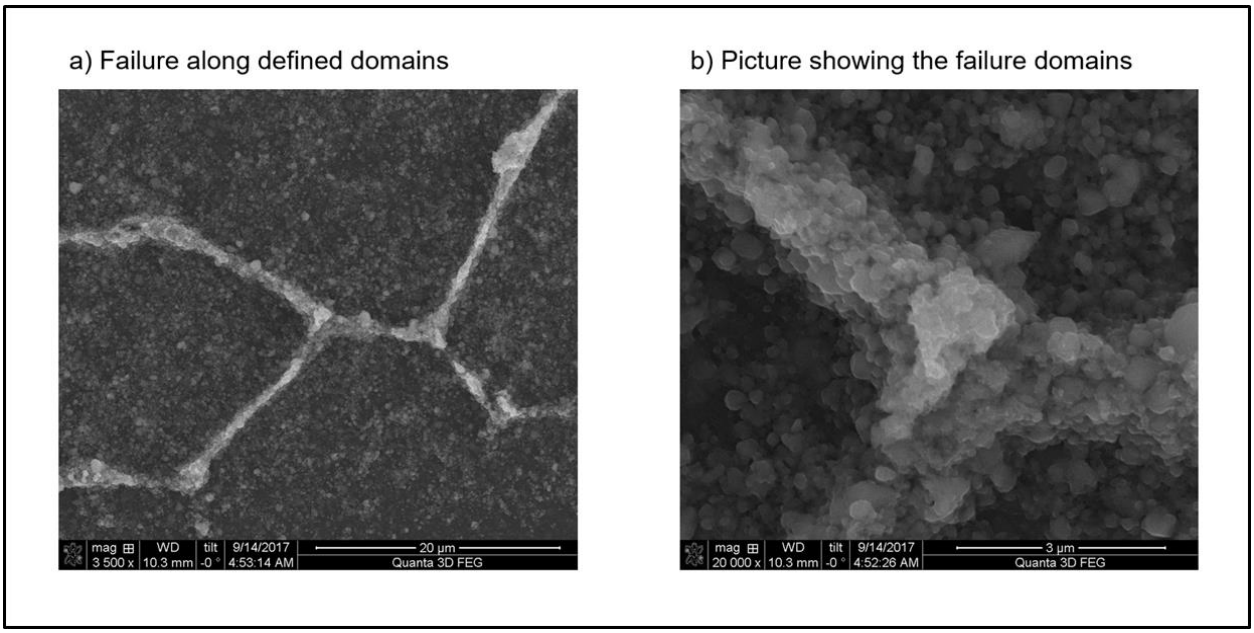

Fig 2.8: Top-down view of the failed bonded interfaces showing failure along defined domain due to incomplete sintering.

2.4. Summary

The commercial nanoparticle ink (provided by Pvnanocell) demonstrated high electrical conductivity and mechanical strength making it extremely suitable for use as electrical interconnect in integrated circuits. However, due to the thermal budgets imposed on circuits today, a sintering temperature of 300 ^{0}C for 1 hour can be extremely detrimental to the reliability of the rest of the package. As a result, alternative copper inks were required to be explored which provided similar electrical and mechanical properties at lower temperatures. Some of these inks have been discussed in subsequent chapters.

Chapter 3. Copper Sol-gels

Solution-processed inks/gels (referred to hereafter as Sol-gels) consists of metal salts that are present in solution with some reducing agent. These inks are then chemically reduced to metal when the solutions are exposed to thermal energy. [15] Sol-gels are extremely useful for printing technologies as they are easy to synthesize and remain stable in air (unlike the commercial copper nanoparticle inks discussed in Chapter 2). Thus, removing the added complication of handling these systems in inert environments. The synthesis of copper sol-gels and their electrical and mechanical characterizations have been discussed in the subsequent sections.

3.1. Synthesis

Copper Sol-gel with Ammonium Hydroxide

It is known that Copper Formate ($C_2H_2CuO_4$) reduces to metallic copper upon exposure to heat. [16] This phenomenon was used to formulate the copper sol-gel inks. Figure 3.1 (a) shows the copper sol-gel ink that was designed using a solution of Copper Formate salt ($C_2H_2CuO_4.2H_2O$) and ammonium hydroxide (NH_4OH) with water as the solvent. In this reaction, water was used as the solvent as both Copper Formate and Ammonium Hydroxide are soluble in it. The ink was formulated by mixing 0.2 g of Copper Formate with a minimum amount of Ammonium Hydroxide (aq). Then, the solution was diluted with water in order bring the ink within the jettability window for inkjet printing. Fig 3.1 (a) shows the primary chemical reaction while Fig 3.1 (b) illustrates the intermediate steps of the chemical reaction that the system undergoes upon exposure to heat to reduce the copper salt to copper metal. As shown in the figure, after the completion of the reaction, ammonia gas is expelled from the system leaving behind pure copper. This expulsion of ammonia during the conversion process resulted in porous films leading to poor mechanical strengths of the films as will be discussed in Section 3.4.

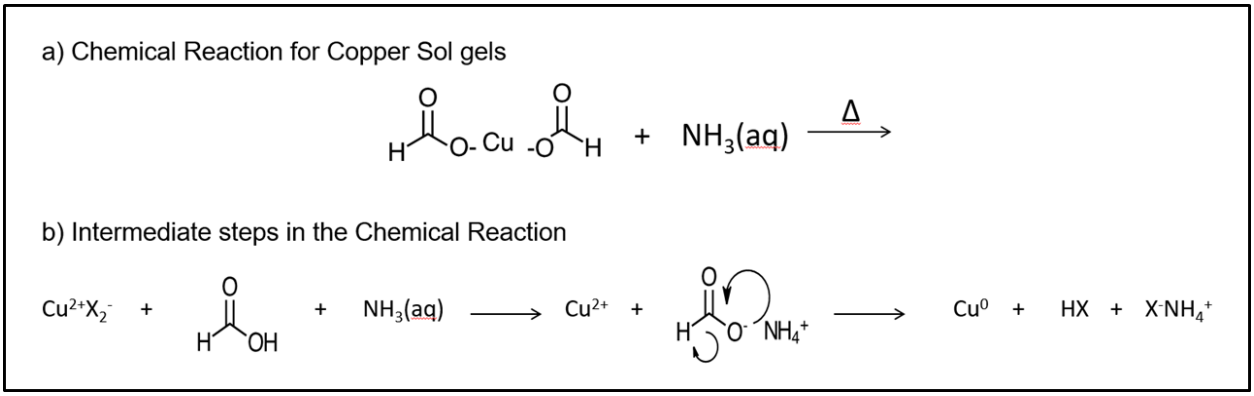

Fig 3.1: (a) Chemical reaction showing the chemicals used for the Copper sol-gels, (b) Intermediate steps in the reaction showing the conversion of copper salt to copper metal.

In order to mitigate the issues discussed above, another formulation for the sol-gels was conceived in which the Copper Formate salt was mixed in Amino methyl propanol (Fig. 3.2). [17] Amino methyl propanol, having a higher boiling point (165 ^{0}C) than Ammonium hydroxide (24.7 ^{0}C), does not leave the solution at room temperature. As a result, this mixture did not release ammonia gas as a byproduct, making the films much smoother than the previous sol-gel formulation. This ink was designed by mixing 1 g of Copper Formate with 10 mL of Amino methyl propanol. This solution was then diluted with 10 mL of Butanol and an appropriate amount of 2-(2-Butoxyethoxy) ethanol to tune the surface tension to be within the jettability window for inkjet printing.

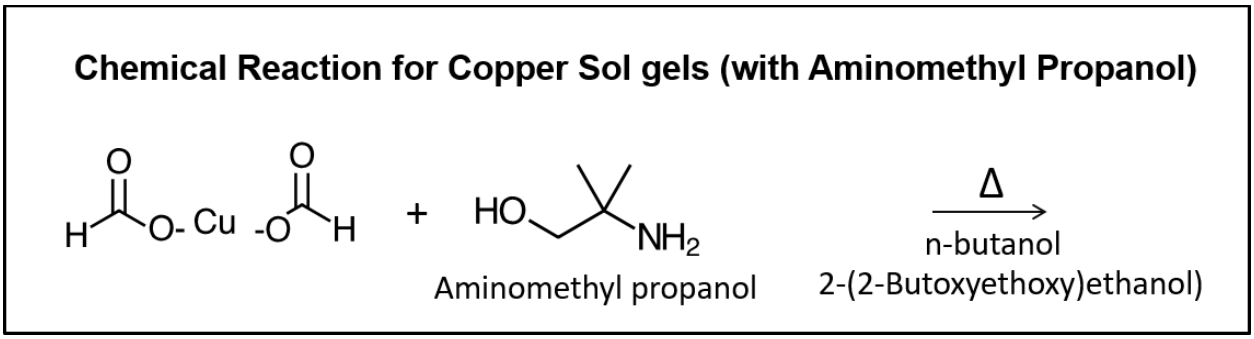

Fig 3.2: Chemical reaction showing the formulation of copper sol-gel using Amino methyl propanol as a reducing agent.

3.2. Printing of Copper Sol-gels

The copper salt (Copper Formate) and the binding agent (Amino methyl propanol) by itself were sufficient for conversion to copper metal. However, to form printable ink, several solvents and thinning agents were added to it. These modifications of fluid properties and jetting waveform to obtain reliable drops during printing have been discussed in this section.

3.2.1. Ink Formulation

As discussed in Chapter 1, the first task is ink design is to formulate an ink such that its fluid properties fall within the jettability window for inkjet printing. In this experiment, different alkoxy alcohols (2-(2-Butoxyethoxy ethanol), 2-Methoxyethanol, 2-(2-Methoxyethoxy) ethanol) were mixed with Butanol to tune the surface tension of the ink. The results are shown in Figure 3.3. The x-axis shows the percentage of the surfactant in the solvent mixture, the rest being Butanol while the y-axis shows the resulting surface tension of the solvent mixtures. The upper limit recommended for Fujifilm Dimatix inkjet printers (the inkjet printer used for our experiments) is 60 mN/m. As a result, only the inks diluted with 2-(2-Butoxyethoxy ethanol) were viable for inkjet printing. The remaining of the experiments used a 25% solvent mixture of 2-(2-Butoxyethoxy ethanol) in Butanol as it allowed for the maximum mass loading for a given volume of ink.

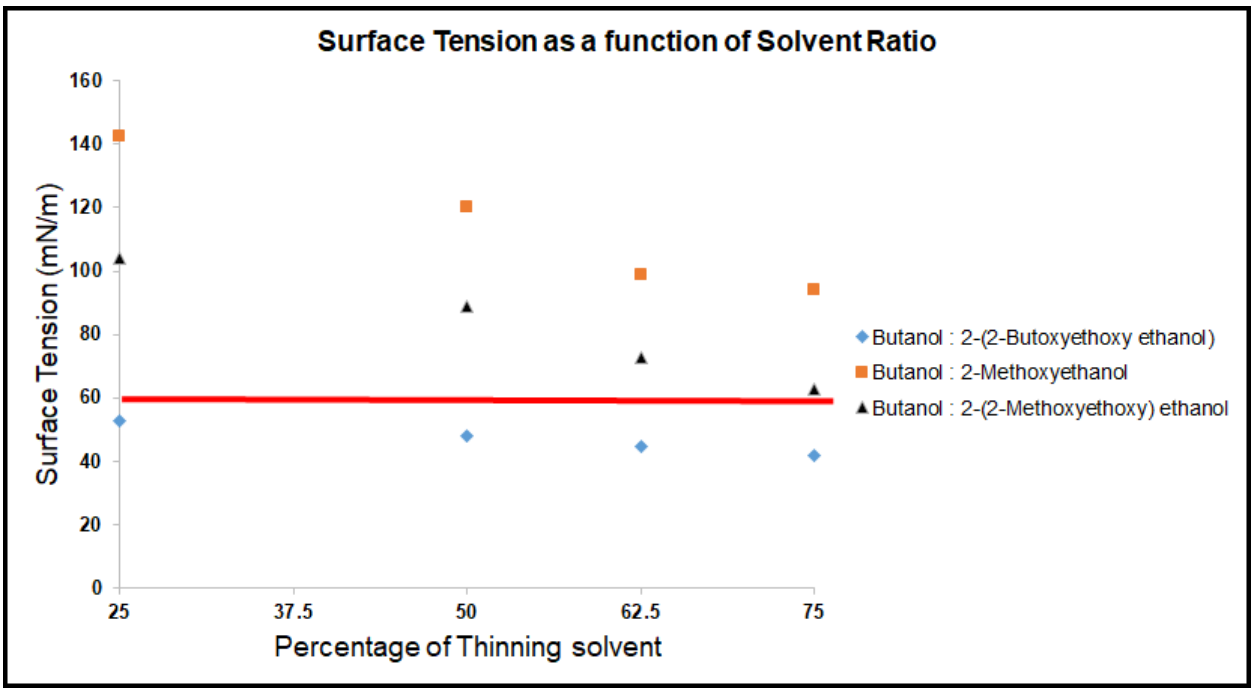

Fig 3.3: Surface Tension as a function of percentage of surfactant in the solvent mixture (the rest being butanol). The red line indicates the recommended upper limit of surface tension for inks printed with the Fujifilm Dimatix Inkjet printers.

3.2.2. Inkjet Printing of Copper Sol-gels

An extended jetting experiment was conducted to determine the printability of the copper sol-gels. The ink used for the study, as mentioned previously, was a mixture of 25% 2-(2-Butoxyethoxy ethanol) and 75% copper sol-gel solution mixed in Butanol by volume. The factors for the experiment were Dwell time, Rise/Fall time, Voltage, Head temperature and Meniscus pressure while printability was determined by the consistency of the ejected drops and the presence/absence of satellite drops. Figure 3.4 shows the waveform that provided the most consistent drops. In this waveform, the fall time (2 μs) turned out to be twice the rise time (1 μs) while the negative pulse voltage (V_2) was determined to be equal in magnitude but opposite in sign to the positive pulse voltage (V_1). The head temperature, meniscus pressure and jetting frequency were 45 ^{0}C, 4.5 mm of Hg and 1 kHz respectively.

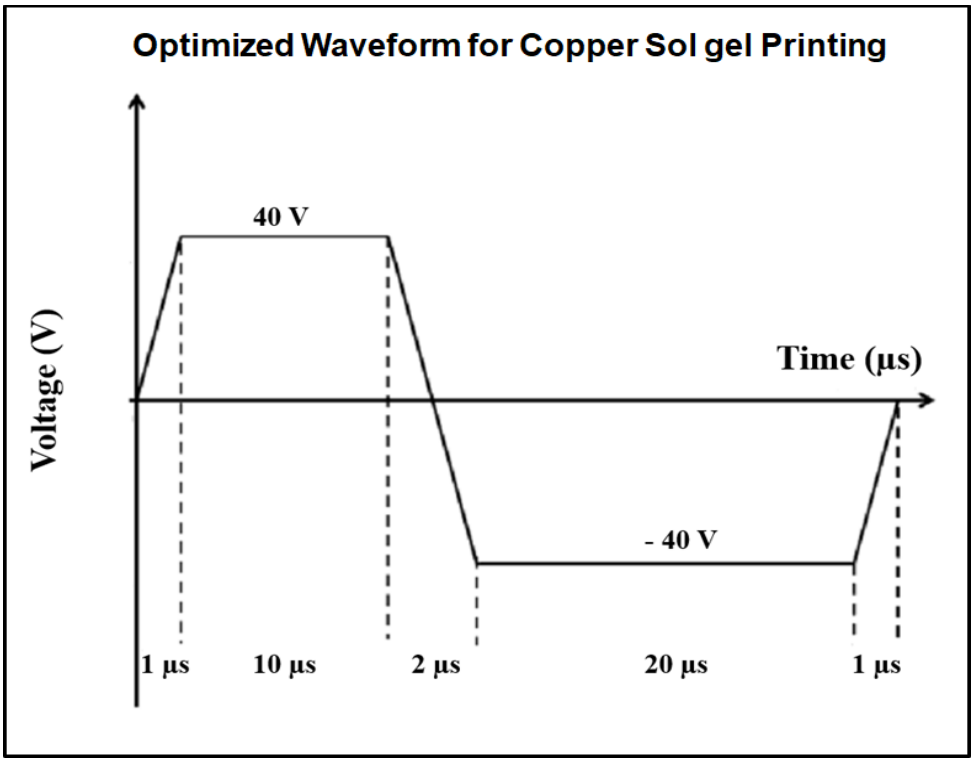

Fig 3.4: The optimized waveform for Copper sol-gel printing showing the various waveform parameters.

3.3. Electrical Characterization of Printed Sol-gels

The graph below (Fig. 3.5) shows the electrical resistivity of both the copper sol-gel formulations (containing Ammonium hydroxide and Amino methyl propanol) as a function of sinter temperature. These experiments were conducted in air and the sintering time was 1 hour for each sample. As can be seen from the plot, these inks exhibited a resistivity close to ten times the resistivity of bulk copper at temperatures as low as 150 ^{0}C. This was significantly lower than the temperature required for the sintering of the commercial nanoparticle ink which, as discussed previously, was 300 ^{0}C. As a result, they provided a viable option for replacement of eutectic solders with copper in electronic packaging applications as they fall within the thermal budgets of the integrated circuit.

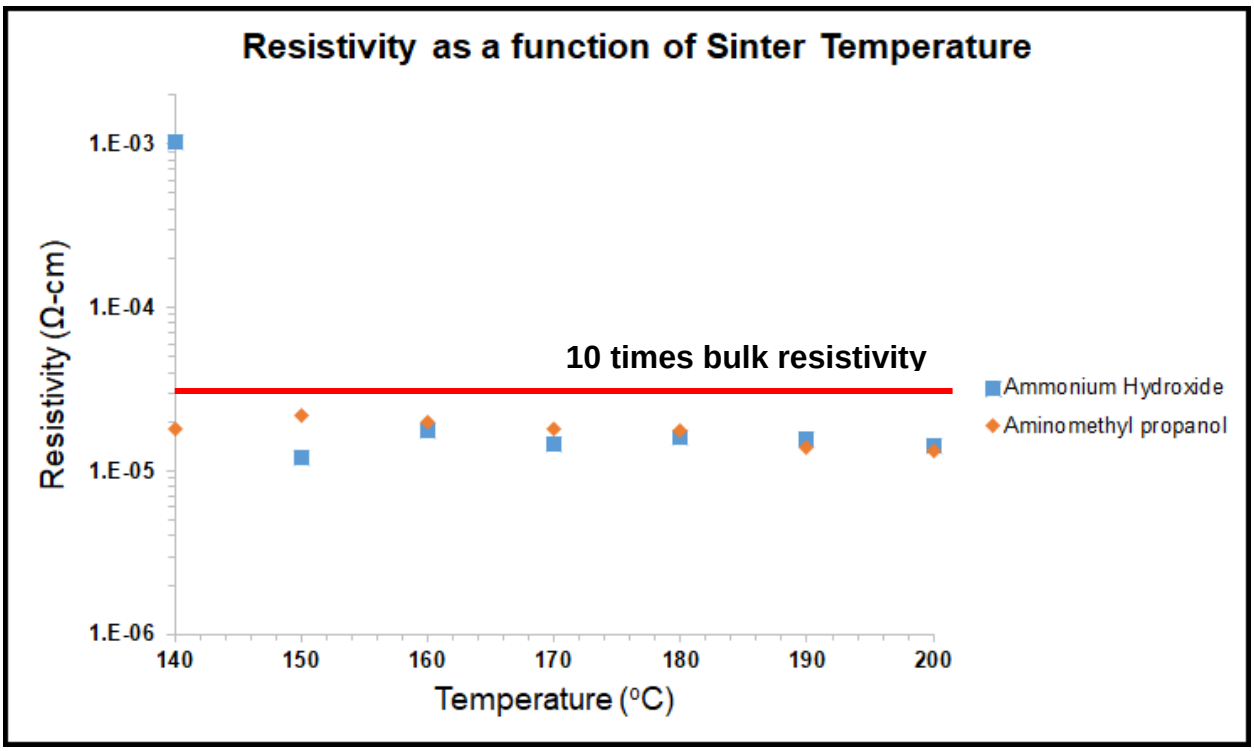

Fig 3.5: Sintering study of the two Copper sol-gel formulations showing resistivity as a function of sinter temperature.

3.4. Mechanical Characterization of Printed Sol-gels

The experimental setup for the mechanical testing of the printed copper sol-gels was similar to the one described for the commercial nanoparticle inks (Section 2.3). As a reminder, it involved printing of an array of copper sol-gel onto an evaporated copper substrate. The length, width and height of each printed line was 1 cm, 150 µm and 1.5 µm respectively with a pitch of 0.5 mm covering a total area of 1 cm^2. Then, a copper die was placed upside down on top of the printed surface and was flip-chip bonded (using a Finetech Flip Chip Bonder) under the application of a defined force. Following that, the samples were heated at 200 ^{0}C for 1 hour. The entire bonding and sintering process was done in air. Finally, a bond tester (Mbraun Bond Tester) was used to apply a shear force on the bonded region to study mechanical strengths of the structures.

The results of the bonding study are presented in Figure 3.6. As expected, the shear strengths of the bonds increased with increasing applied force. However, the bonds formed by the copper sol-gels were an order of magnitude lower in strength than those obtained from the printed commercial nanoparticle inks (shear strength = 1.1×10^4 g/cm^2). More importantly, they were a couple order of magnitude lower than the strengths reported for the state of the art eutectic solders (shear strength = 210.09 kg/cm^2).[3] These weak bonds were likely due to the porous films that were formed during the conversion of copper salt to copper.

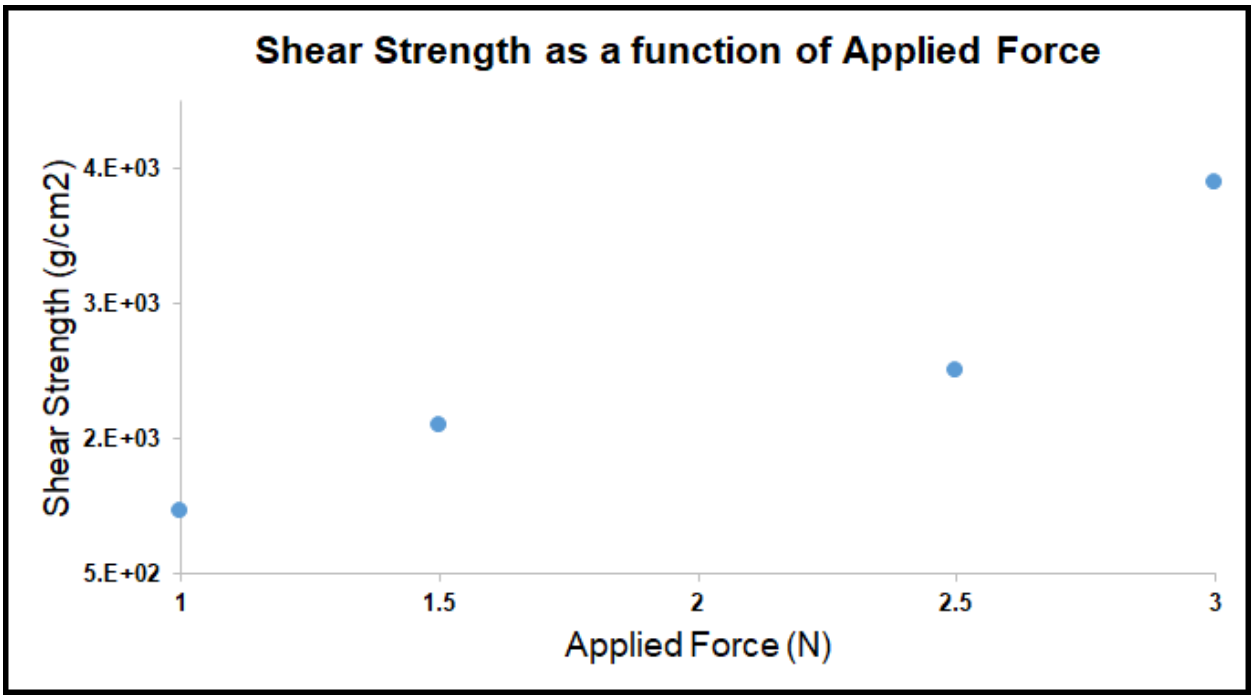

Fig 3.6: Results of bonding study for printed copper sol-gels showing shear strength of the bonded copper sol-gels as a function of applied force.

The following figure (Figure 3.7) shows the resulting films of the copper sol-gels after conversion. The films were found to be porous throughout the thickness of the structure. This was likely due to the expulsion of ammonia gas during the conversion process. As a result, this lead to poor mechanical strengths within the bulk of the film leading to low shear strengths. Moreover, an AFM (Atomic Force Microscopy) measurement of the films showed a surface roughness of 362.5 nm which meant that not all the film was able to contact the copper die. As a result, the poor contact between the copper die and the converted copper films could have also resulted in the observed weak bond strengths.

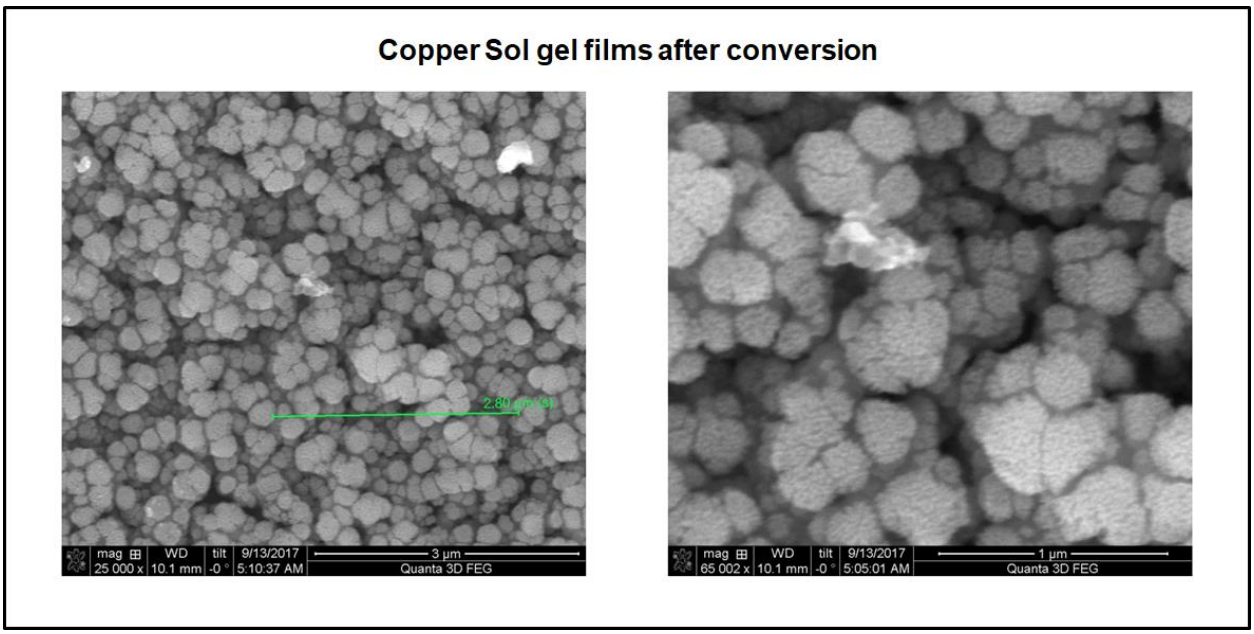

Fig 3.7: Copper sol-gel films after conversion showing the porosity in the films due to the evolution of ammonia gas.

3.5. Summary

The copper sol-gel inks provided a pathway for obtaining highly conductive films at temperatures well below the thermal budget for electronic packaging. Unfortunately, the weak mechanical strengths of the bonds prevent them from being ideal candidates for the replacement of solder with copper. Therefore, other synthesis routes for copper had to be conceived, ideally ones that would provide stable inks, low temperature conversion to copper and high mechanical strength. The following chapter discusses synthesis of an in-house copper nanoparticle ink that gets us a little closer to fulfilling all the requirements.

Chapter 4. In-house Nanoparticle systems (PVP-CTAB Copper Nanoparticles)

As discussed previously, the commercial nanoparticle inks provided highly conductive copper films with high mechanical strengths. However, they were not viable for electronic packaging applications due to their high temperature sintering requirements. In this chapter, an in-house copper nanoparticle synthesis is discussed which allowed us to avoid the high temperature processes. The chemical reaction to make the nanoparticle along with solvents for ink formulation have been discussed. Following that is a discussion of the electrical and mechanical characterization of the resulting films.

4.1. Synthesis

Figure 4.1 shows the chemical reaction used to make the copper nanoparticles. In this reaction, 0.5 g of Copper Sulfate salt, 0.35 g of Cetrimonium Bromide (henceforth referred to as CTAB) and 0.4 g of Polyvinyl pyrrolidine (PVP) were dissolved in 20 mL of Ethylene glycol. The reaction mixture was allowed to dissolve at 80 ^{0}C. Then, 20 mL of 1.6 M hydrazine hydrate was slowly injected into the solution at this temperature. This served as the reducing agent to reduce copper sulfate salt into copper. The reactants were allowed to react at 80 ^{0}C for half an hour. Then, the solution was cooled down to room temperature and stirred for 2 hours. The particles were then separated by centrifuging the solution and washing with ethanol. This process of separation was repeated 3 times to remove the residual solvents from the system. This synthesis was based on work done by *Athawale*, *Katre, Kumar* and *Majumdar.* [18]

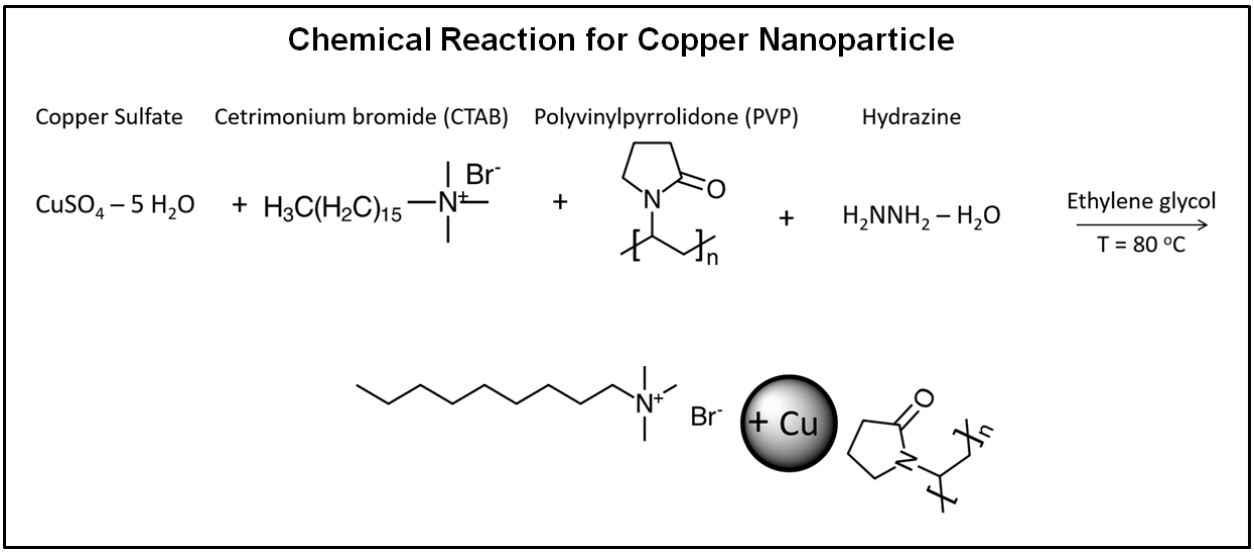

Fig 4.1: Chemical reaction showing the synthesis of copper nanoparticles with PVP/CTAB as the ligands.

In the above reaction, the tertiary amine groups in CTAB along with the PVP act as the surfactant that surround the copper nanoparticles. These particles showed high resistance to oxidation in air. However, they still had to be sintered in inert conditions to prevent the oxidation of the nanoparticles after the ligands had left the system. The hydrazine functioned as the reducing agent for the reaction while Ethylene glycol was used the solvent for the system.

4.2. Printing of PVP-CTAB Copper Nanoparticle Ink

Two printing techniques were used to print the PVP/CTAB copper nanoparticles i.e. inkjet printing and stencil printing. The following sections discuss the solvent study used to determine printable inks for inkjet printing and the issues encountered with them. Following that is a discussion of the stencil printing technique which was eventually used to deposit these particles.

4.2.1. Ink Formulation for Inkjet Printing

The PVP/CTAB Copper nanoparticles contained Ethylene glycol as the primary solvent. However, the solution by itself was not sufficient to form printable inks as their fluid properties lay outside the jettability window for inkjet printing. As a result, Ethanol and Isopropyl alcohol (IPA) were used as thinning solvents to tune the surface tension and viscosity of the inks. In these experiments, the copper nanoparticle inks (with ethylene glycol as the solvent) were diluted with the thinning solvents and the resulting fluid properties were measured. The results are shown in Figure 4.2 and 4.3. The red lines in figure 4.2 indicate the recommended window for the viscosities of the inks printed by the Fujifilm Dimatix inkjet printers (printer used for our experiments) while the red line in figure 4.3 shows the upper limit for the surface tension of the inks printed by the same printer.

As can be seen from the graphs, a 90% solution of the nanoparticle (mixed with ethylene glycol) diluted with 10% ethanol fell within the limits imposed for both viscosity and surface tension. More importantly, this dilution allowed for maximum mass loading in our inks by maximizing the amount of nanoparticle solution present in the ink. As a result, this combination was used to formulate inks for our jetting studies which have been discussed next.

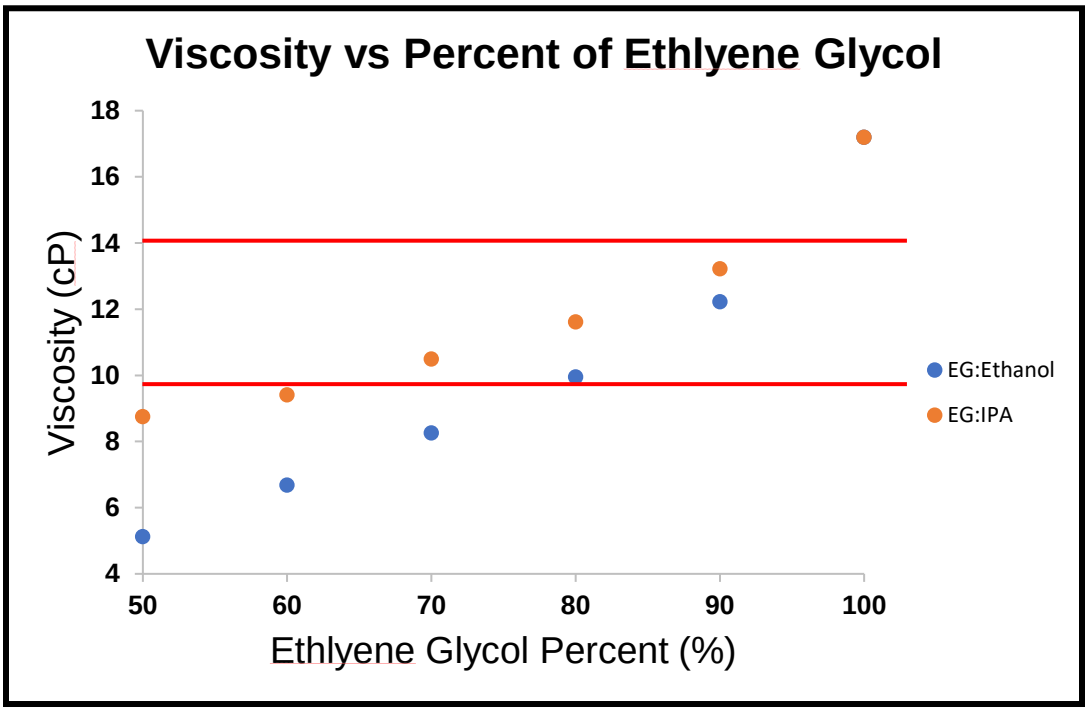

Fig 4.2: Viscosities of inks as a function of percentage of nanoparticle solution present in the ink.

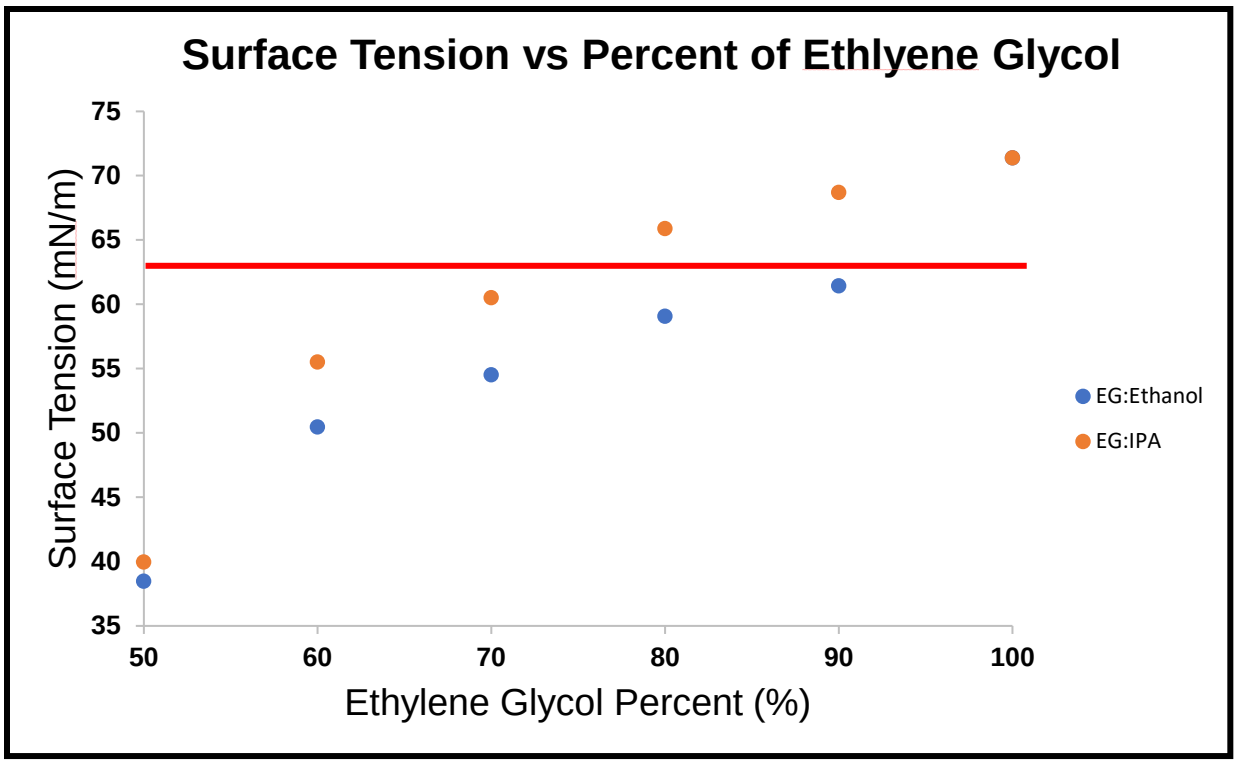

Fig 4.3: Surface tension of inks as a function of percentage of nanoparticle solution present in the ink.

The jetting experiments used to determine inkjet printability of the above inks was similar to the one performed for the copper sol-gels. As mentioned above, the ink used for the study was a 90% solution of copper nanoparticle (mixed with ethylene glycol) mixed with 10% ethanol by volume. The factors for the experiment were Dwell time, Rise/Fall time, Voltage, Head temperature and Meniscus pressure while printability was determined by the consistency of the ejected drops and the presence/absence of satellite drops. Similar to the copper sol-gel experiment, an optimized waveform was generated. Figure 4.4 shows the resulting printed lines after deposition.

Unfortunately, one of the issues encountered during inkjet printing was that jetting through the inkjet nozzle could not be sustained for a long period of time. This was determined to be due to aggregation of the nanoparticles upon drying. An AFM (Atomic Force Measurement) of the deposited sample showed that the surface roughness of the film was 410.83 nm. As can be seen from the images below, this was due to the aggregates present in the film which were much larger in size than the orifice of the nozzle (which was about 0.1 µm). As a result, they clogged the nozzle over time leading to inconsistent drop ejection and eventual blockage. These issues with inkjet printing were hard to overcome with this system and therefore stencil printing was considered as an alternative printing technique to deposit these particles. This has been discussed in the next section.

4.2.2. Stencil Printing of PVP-CTAB Copper Nanoparticle Inks

The stencil printing process of the PVP/CTAB copper nanoparticles has been shown in Fig. 4.4. Since stencil printing is a simple deposit and drag process, the limitations on the fluid properties are less stringent. As a result, the initial copper nanoparticle solution containing ethylene glycol as the solvent was sufficient to formulate inks for stencil printing. As shown in the figure, the first step in the printing process was to place a mask over the copper substrate with a pattern over which the ink could be transferred. After the ink was deposited over the entire mask, a doctor blade was used to wipe out the unused ink, leaving behind a uniform layer of the copper nanoparticle ink. The sample was then dried or sintered according to the requirements of the experiment. The thickness of the film was controlled by adjusting the height of the mask. One things to note about these samples is that the aggregation of particles discussed in the previous section were still visible in the dried films. However, they were not an issue with stencil printing as the patterns on the mask were much larger than the size of the aggregates.

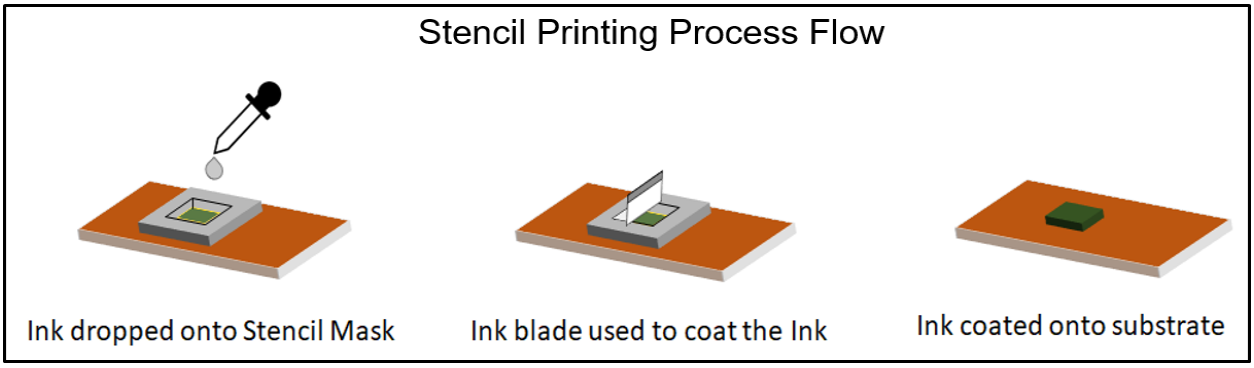

Fig 4.4: Schematic showing the stencil printing process flow for PVP/CTAB copper nanoparticles.

4.3. Electrical Characterization of PVP-CTAB Copper Nanoparticles

The electrical resistivity of the copper nanoparticle films as a function of sinter temperature has been shown in Figure 4.5. These experiments were conducted in a nitrogen environment and all the samples were sintered for 1 hour at their respective temperatures. As can be seen from the graph below, the PVP/CTAB copper nanoparticles exhibited a resistivity close to ten times the bulk resistivity of copper at 200 ^{0}C and higher. Although it is slightly higher than the temperatures discussed for copper sol-gels, it is significantly lower than the temperatures required to sinter the commercial copper inks (discussed in Chapter 2). More importantly, 200 ^{0}C is well within the thermal budgets for integrated circuits, thus making this system extremely viable for solder replacement applications in those systems.

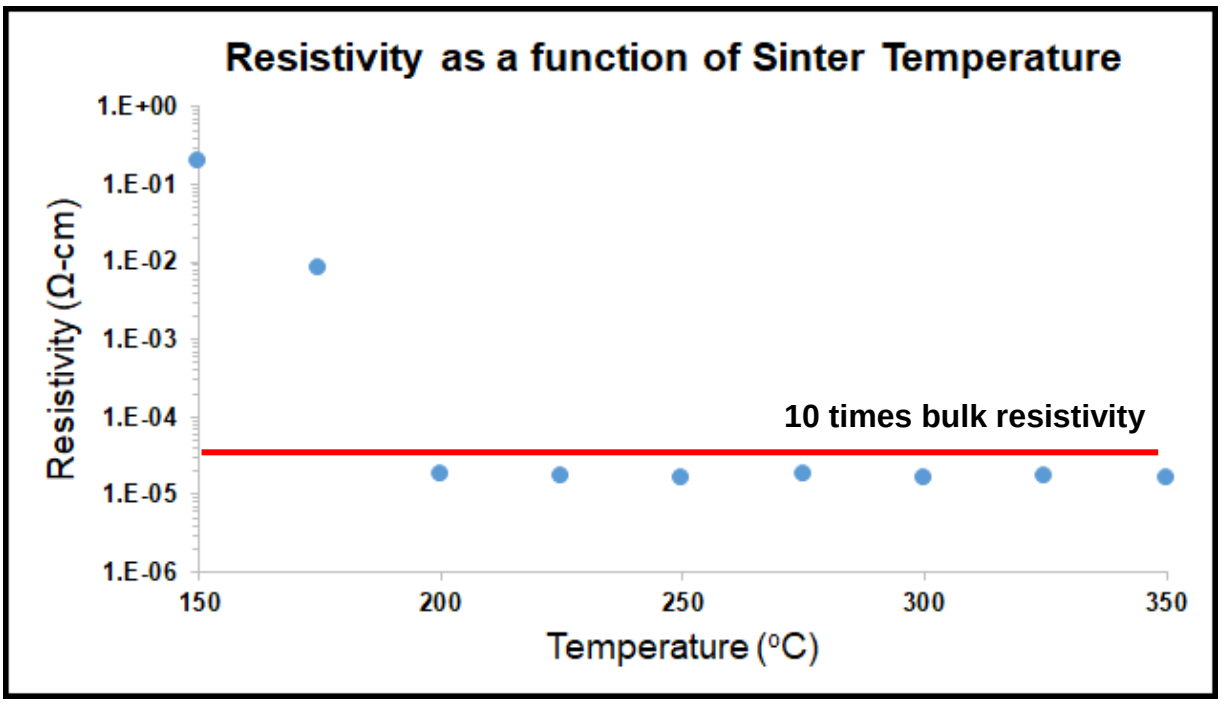

Fig 4.5: Sintering study of PVP/CTAB Copper nanoparticle ink showing electrical resistivity as a function of sinter temperature.

4.4. Mechanical Characterization of Printed Copper Nanoparticles

The experimental setup for the mechanical testing of printed PVP/CTAB copper nanoparticle structures was similar to the one described in the commercial copper nanoparticle ink chapter (Chapter 2). As a quick reminder, it involved printing of an array of copper nanoparticles onto an evaporated copper substrate. The length, width and height of each printed line was 1 cm, 150 µm and 1.5 µm respectively with a pitch of 0.5 mm covering a total area of 1 cm^2. Then, a copper die was placed upside down on top of the printed surface and was flip-chip bonded (using a Finetech Flip Chip Bonder) under the application of a defined force. Following that, the samples were heated at 200 ^{0}C for 1 hour. The entire bonding and sintering process was done in a nitrogen environment. Finally, a bond tester (Mbraun Bond Tester) was used to apply a shear force on the bonded region to study mechanical strengths of the structures.

The results of the mechanical tests are presented in Figure 4.6. As shown in the graph, the bond strengths increased with increasing applied force. This was expected due to stronger binding of the copper nanoparticles to the evaporated copper surface at higher applied force. However, the bond strengths of the printed structures were significantly weaker than the previously discussed sol-gels and commercial nanoparticles; and more importantly, three orders of magnitude weaker than the strengths reported for the state of the art eutectic solders (shear strength = 21.09 kg/cm^2). As a result, this system failed to meet the mechanical strength criteria that is required for replacement of solder in integrated circuits.

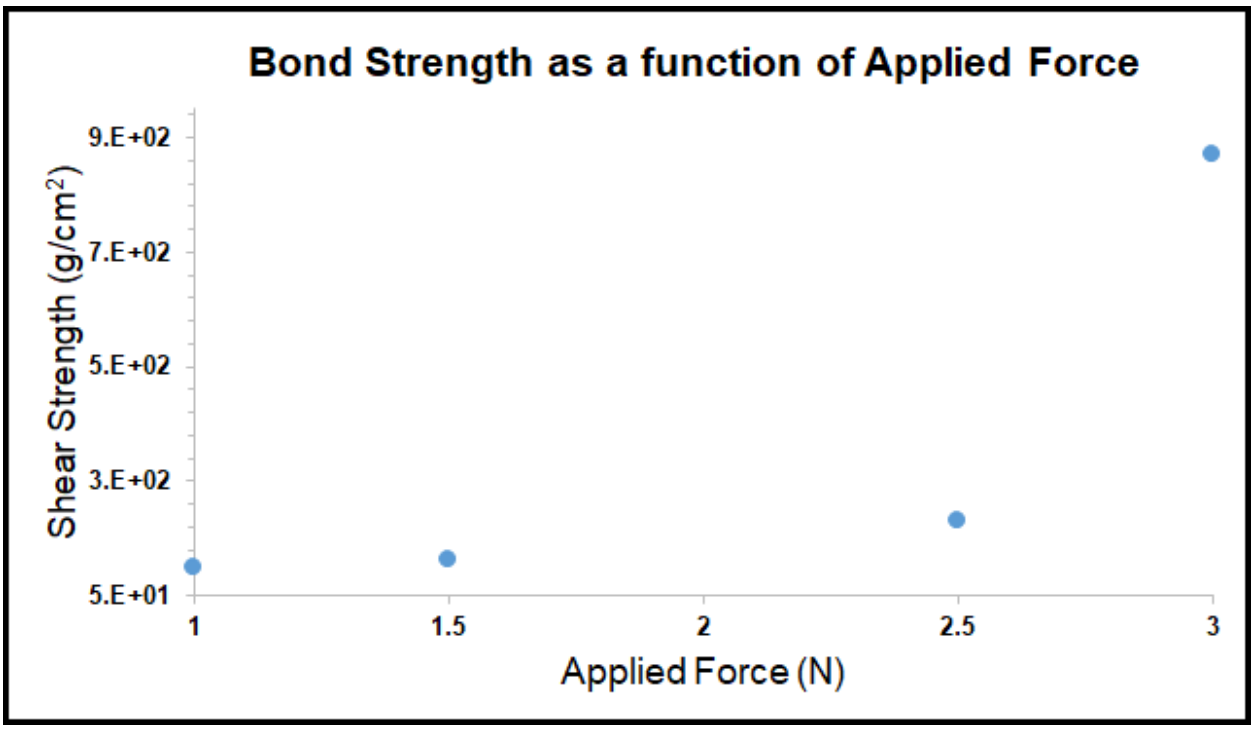

Fig 4.6: Results of bonding study for printed PVP/CTAB copper nanoparticles showing shear strength of the bonded nanoparticles as a function of applied force.

An analysis of the post-bonded structures was done and it was determined that the high degree of roughness on the printed nanoparticle films prevented them from forming intimate contact with the copper dies. Figure 4.7 shows the aggregation of particles on the sintered nanoparticle films. As was discussed above, the surface roughness of these films was about 410 nm with the largest aggregates being around 1 μm in diameter. As a result, when the copper die was placed on top of these films, only the larger aggregates could contact the surface while the rest of the film remained a slight distance away from the die. This led to poor mechanical contact between the films resulting in weak bond strengths. However, as mentioned earlier, these aggregates were difficult to avoid given the particle-ligand system used here. Thus, either an alternative particle system needed to be explored or a change in processing parameters was required to avoid this issue. The next chapter discusses a route to tune the roughness of the sintered nanoparticle films by adjusting the process parameters which could lead to smoother films and potentially stronger bonds.

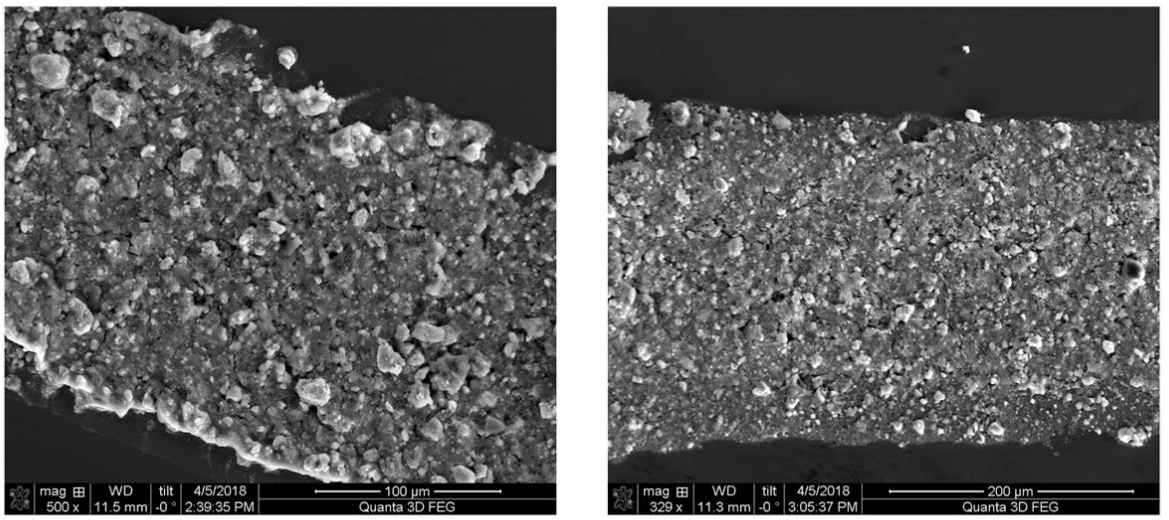

Fig 4.7: PVP/CTAB Copper nanoparticle lines printed by inkjet printing showing the aggregates that eventually inhibit drop ejection through a nozzle.

4.5. Summary

In this chapter, the synthesis of an in-house copper nanoparticle was discussed. The particles provided highly conductive films at temperatures around 200 ^{0}C which was well within the thermal budget for integrated circuit manufacturing. However, the weak mechanical strengths of the bonds made them difficult to be considered for replacement of solder with printed copper. These low strengths were alluded to be due to the poor contact between the die and the nanoparticle film. In order to overcome the problem, the following chapter discusses a metric which can be used to tune the roughness of the sintered films and consequently alter their mechanical strengths.

Chapter 5. Tuning of Mechanical Properties of Nanoparticle Films with Sintering Conditions

Many of the nanoparticles systems that have been discussed in the previous chapters have demonstrated high electrical conductivity at low temperatures but poor mechanical strengths. As a result, a closer look at the sintering conditions were necessary to understand their influence on the mechanical properties of the film. In this chapter, the mechanical strengths of the sintered nanoparticle films were studied as a function of the ramp rate of the temperature profiles during sintering.

5.1. Introduction

As we have seen with our work with copper sol-gels and nanoparticles, film morphology plays a significant role on the overall strengths of the bonded features. As a result, it was important to study the effect of the nanoparticle composition and processing parameters on the final film morphology. In this chapter, the mechanical strengths of sintered silver nanoparticle films were studied as a function of the ramp rate of the temperature profiles during sintering. Silver nanoparticles were chosen for this experiment over copper due to the ease of working with the system i.e. silver nanoparticles are more resistant to oxidation than copper. This simplified the system and helped develop an understanding towards the nature of growth of the nanoparticles.

The organization of the chapter is as follows: the experimental setup for the sintering process will be discussed first. This will be followed by the presentation of the resulting film properties which include the mechanical strengths and morphologies of the nanoparticle films after sintering. In the explanation section, first, a brief literature review is presented which outlines the different nanoparticle growth mechanisms and the phenomenon that are known for the current system. Finally, the chapter will end with an attempt to use the existing knowledge to explain the evolution of the films during the sintering process. This will, in turn help in understanding the role that stabilizing ligands play to influence the final morphology and strength of the sintered nanoparticle films.

5.2. Experimental Section

The following figure (Fig. 5.1) shows the process flow for the experiment. In this investigation, silver nanoparticles having an average diameter of 4 - 5 nm were synthesized using the synthesis techniques developed by *Wu, Li and Ong*. [7], [19] Dodecyl amine ($C_{12}H_{27}N$) was used as the ligand to protect the nanoparticles from aggregating while Dodecane ($C_{12}H_{26}$) was used as the solvent to transfer the particles. Again, as mentioned above, Silver nanoparticles were chosen for this experiment over copper due to their resistance to oxidation in air. This simplified the system and helped develop an understand towards the nature of growth of the nanoparticles. Dodecane was used as the solvent as these nanoparticle systems are most soluble in this solvent providing a high mass loading of 70 - 80 %.

After the ink was formulated (Silver nanoparticles + Dodecane), the particles were transferred onto an Silicon dioxide (SiO_2) wafer using a stencil printing technique. The films were then dried in a vacuum chamber at 200 mTorr for 5 minutes to remove the excess solvent present in the system. The thickness of the films upon drying were carefully controlled to be between 700 - 800 nm. Following that, the samples were heated on a hot plate to 300 ^{0}C at different ramp rates (^{0}C/minute). Finally, once the sample preparations were over, a Bruker Nanoindenter (Hysitron TI 950) was used to perform nanomechanical testing on the sintered films. The resulting Young's modulus for the films are discussed in the next section.

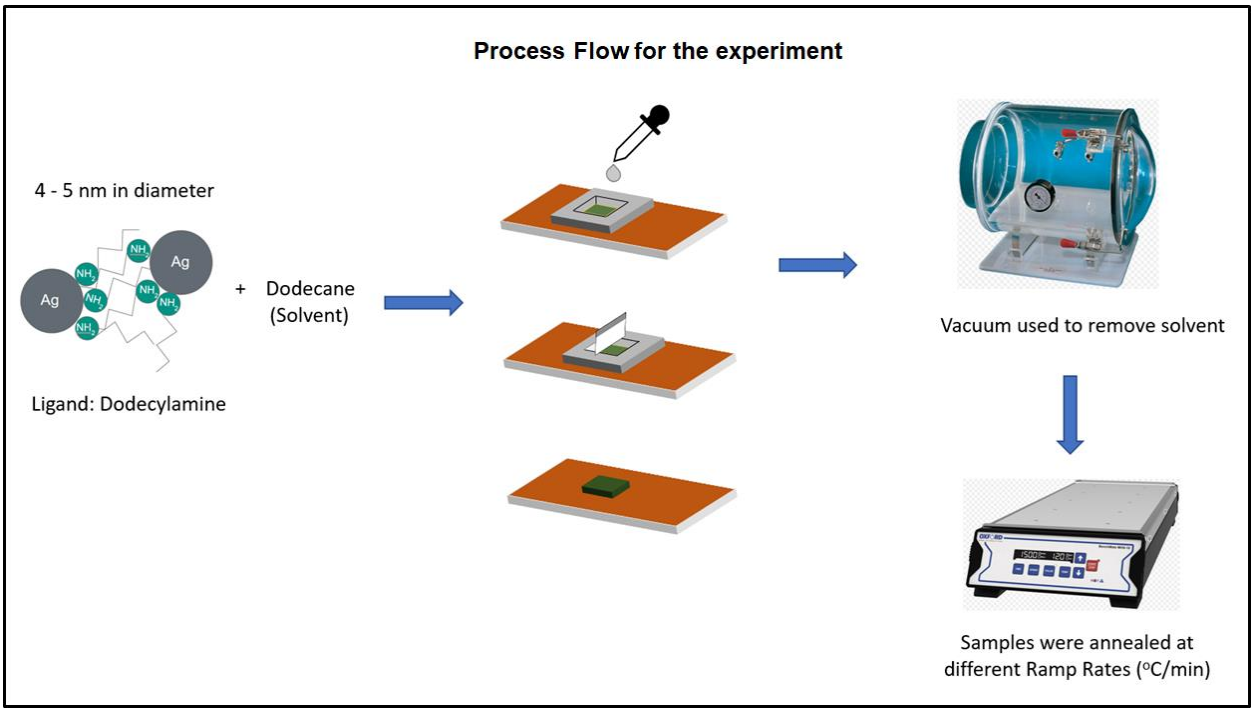

Fig 5.1: Schematic showing the process flow for the silver film sample preparation used for mechanical testing.

5.3. Results

The graph below (Fig. 5.2) shows the mechanical strengths of the sintered films (determine in terms of their Young's modulus) as a function of the temperature ramp rate (^{0}C/minute) on the sintering profile. As mentioned in the previous section, the initial and final temperatures of the profile were 25 ^{0}C and 300 ^{0}C respectively. Furthermore, it is important to mention that the samples were removed immediately after the profile reached 300 ^{0}C i.e. the samples were not kept at 300 ^{0}C for any defined amount of time and were removed within a few seconds of reaching that temperature. As can be seen from the graph below, the mechanical strengths of the films increased dramatically by increasing the ramp rate of the temperature profile. This, as will be discussed in the next section, was due to the competing nature between densifying and non-densifying growth mechanisms which ultimately result in different film morphologies.

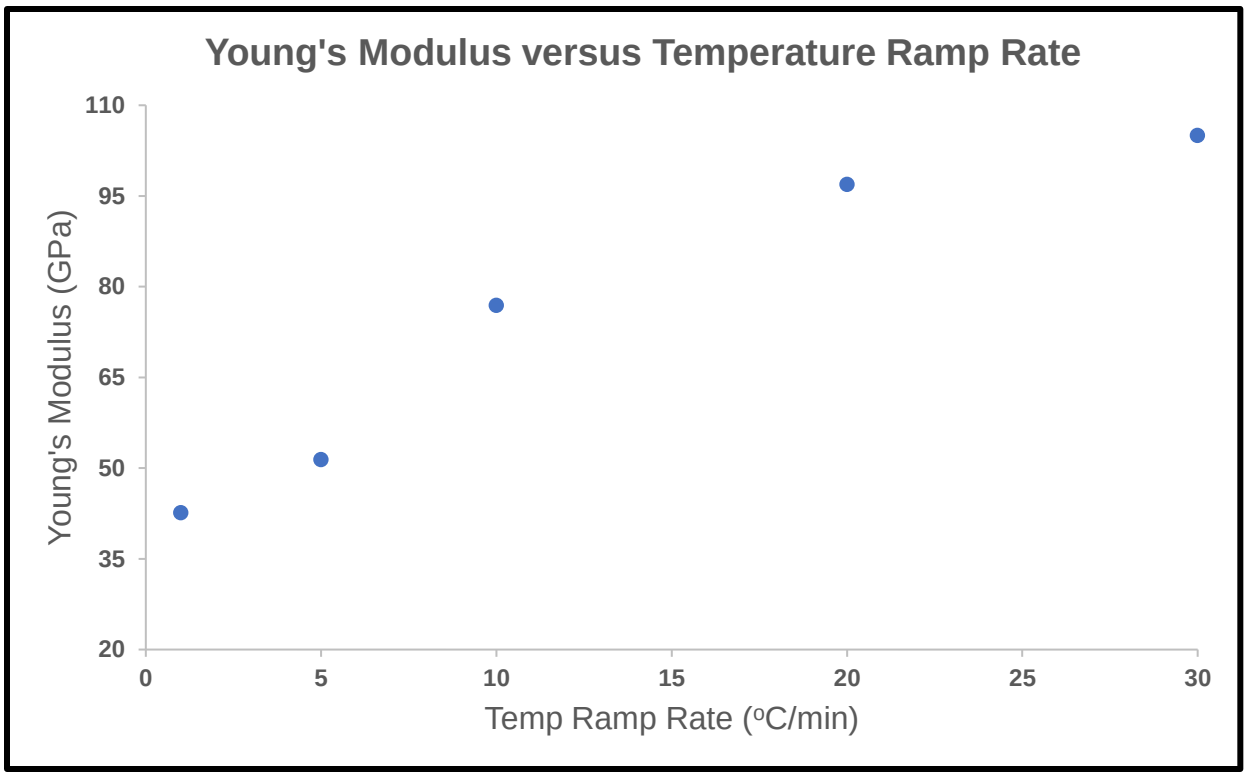

Fig 5.2: Results of the mechanical testing of sintered nanoparticle films showing the Young's modulus as a function of the temperature ramp rate. The initial and final temperature being 25 ^{0}C and 300 ^{0}C respectively.

Figure 5.3 shows the SEM (Scanning Electron Microscope) images of two different films sintered at different temperature ramp rates. By looking at the films under the SEM, it was clear that the higher strength in the films come from the higher densification of particles during the sintering process. The film sintered at a ramp rate of 1 ^{0}C/minute had a porous structure with small crystallite sizes while the sample sintered at 30 ^{0}C/minute displayed a denser film with larger crystallite sizes. This difference in morphology can be explained by understanding the growth mechanisms of the nanoparticles during the sintering process.

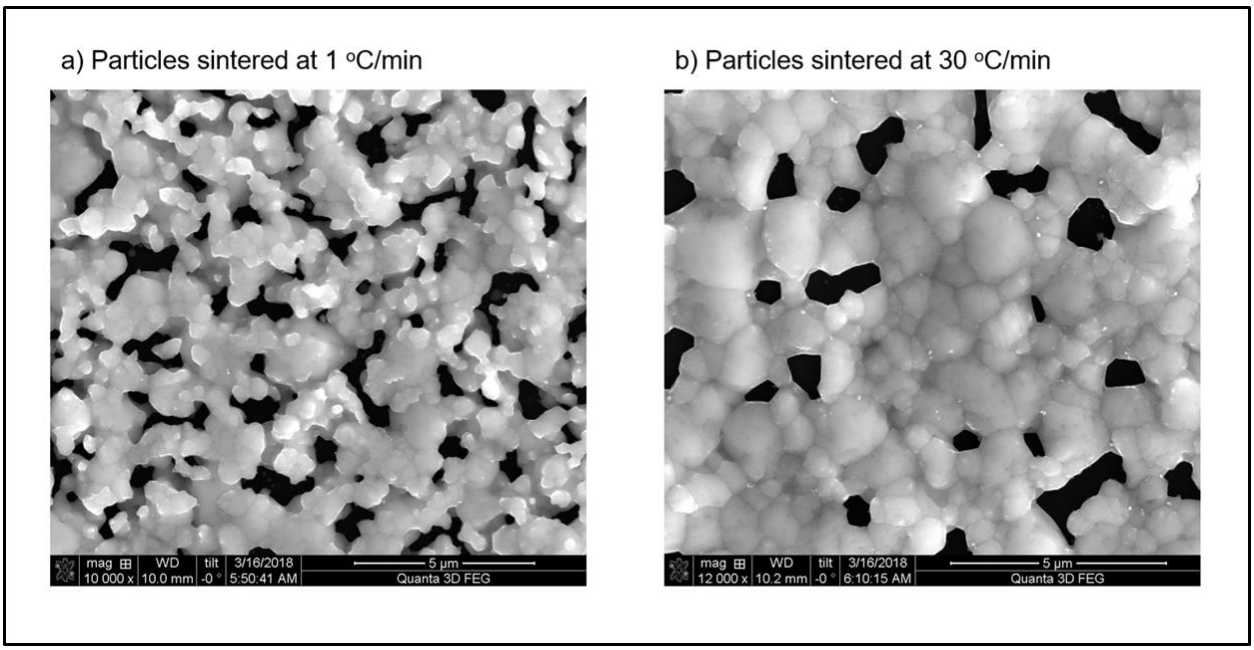

Fig 5.3: SEM images of silver nanoparticle films sintered at (a) 1 ^{0}C/min ramp rate and (b) 30 ^{0}C/min ramp rate.

5.4. Explanation

The observed morphology of the nanoparticle films is consistent with what people have observed for ceramic sintering. As has been explained in the literature for ceramic sintering, mass transport during sintering of two nanoparticles includes surface diffusion, lattice diffusion and grain boundary diffusion. These mechanisms have been schematically represented in Figure 5.4. [9] All of these mass transport mechanisms can be broadly classified into two categories: densifying and non-densifying growth mechanisms. [20] During sintering, these compete to influence the final morphology of the film depending on their ability to cause shrinkage. [21] Both densifying and non-densifying mechanisms lead to a more thermodynamically stable state by reducing the surface area to volume ratio.

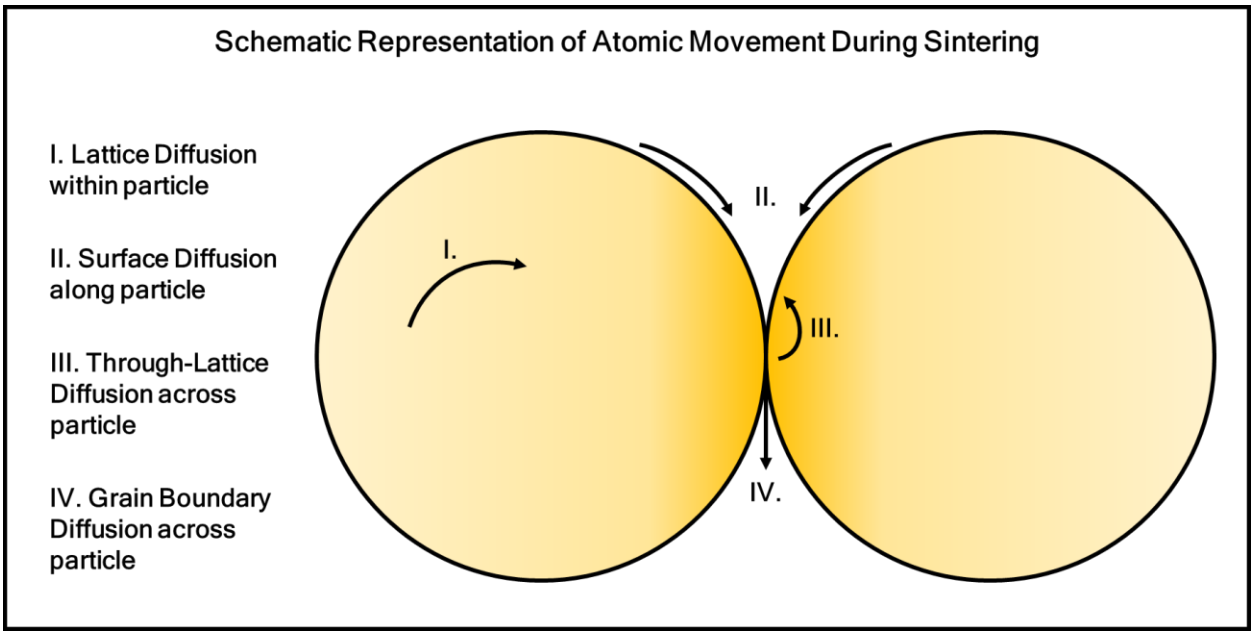

Fig 5.4: Schematic representation of material transport during sintering between two particles.

The non-densifying growth mechanism in silver nanoparticles was first discussed by *Volkman*. In his work, he demonstrated that nanoparticles tend to grow through surface and lattice diffusion in the presence of ligands. [22] This happens through a process known as Oswald's ripening where the ligands function as solvent medium to transport atoms from one nanoparticle to the other. This has been shown schematically in Figure 5.5. This process of nanoparticle growth (namely Oswald's ripening) leads to the initiation of a neck formation between particles and subsequent neck growth upon more atom transfer. This is what we observed in the films that were sintered at a slower ramp rate (Figure 5.3 (a)). While on the other hand, in the absence of these ligands, particles cannot undergo surface diffusion and as a result, they grow through grain boundary diffusion and through-lattice diffusion. This causes volume shrinkage leading to coalescence of the nanoparticles as shown in Figure 5.6. Nanoparticle systems undergoing grain boundary diffusion lead to a denser film and thus the mechanism of growth is termed as densifying growth. This is observed in films that were sintered at a faster ramp rate (Figure 5.3 (b)).

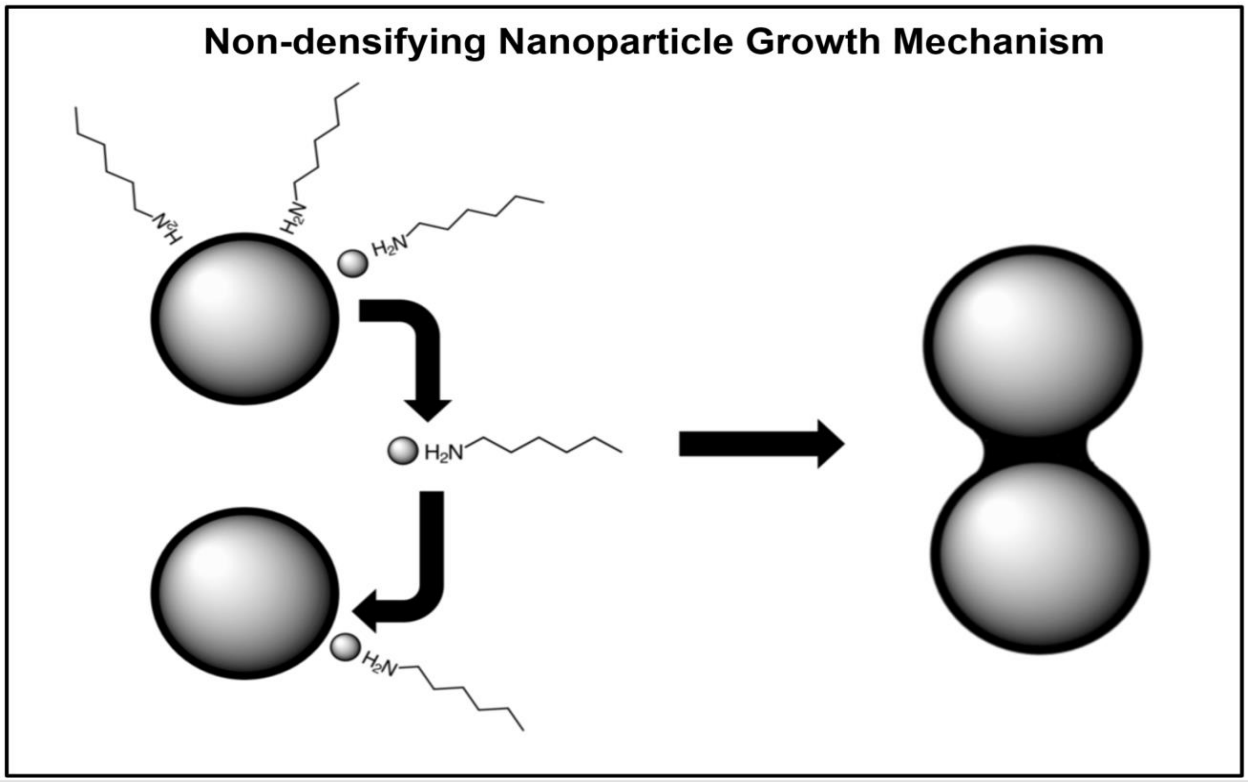

Fig 5.5: Schematic representation of the Non-densifying growth mechanism sintering between two particles in the presence of ligands.

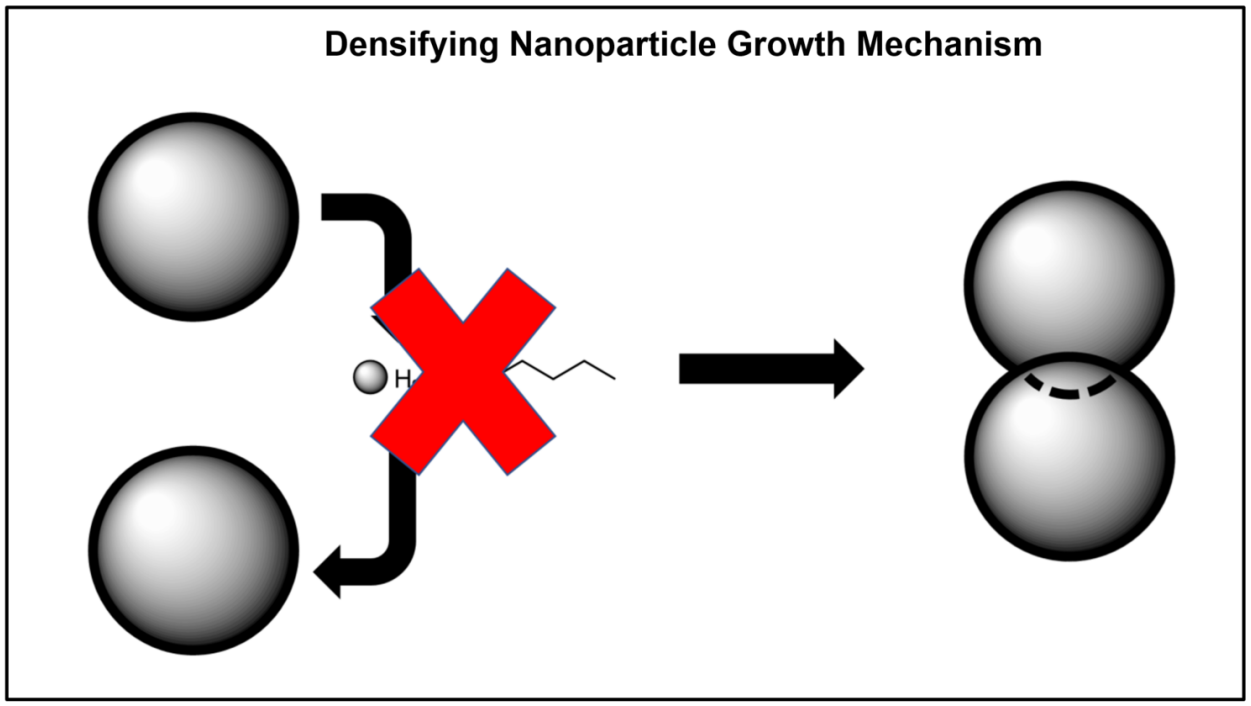

Fig 5.6: Schematic representation of the inability of the nanoparticle to undergo surface diffusion in the absence of ligands leading to densifying growth between particles.

It is known that sintering in dodecyl amine encapsulated silver nanoparticle systems occur in the presence of some residual ligands which get trapped within the bulk of the film. [23] Previous studies have also shown that although the temperature at which the dodecyl amine starts to dissociate from the nanoparticles is about 150 ^{0}C, the films begin to demonstrate conductivity at around 120 ^{0}C indicating some sintering. This is illustrated by the TGA (Thermogravimetric Analysis) data (Figure 5.5) which shows mass loss beyond 150 ^{o}C indicating the presence of residual ligand in the system. As a result, given our understanding of the different growth mechanisms during sintering, we can now discuss the difference in morphologies of the sintered nanoparticle films.

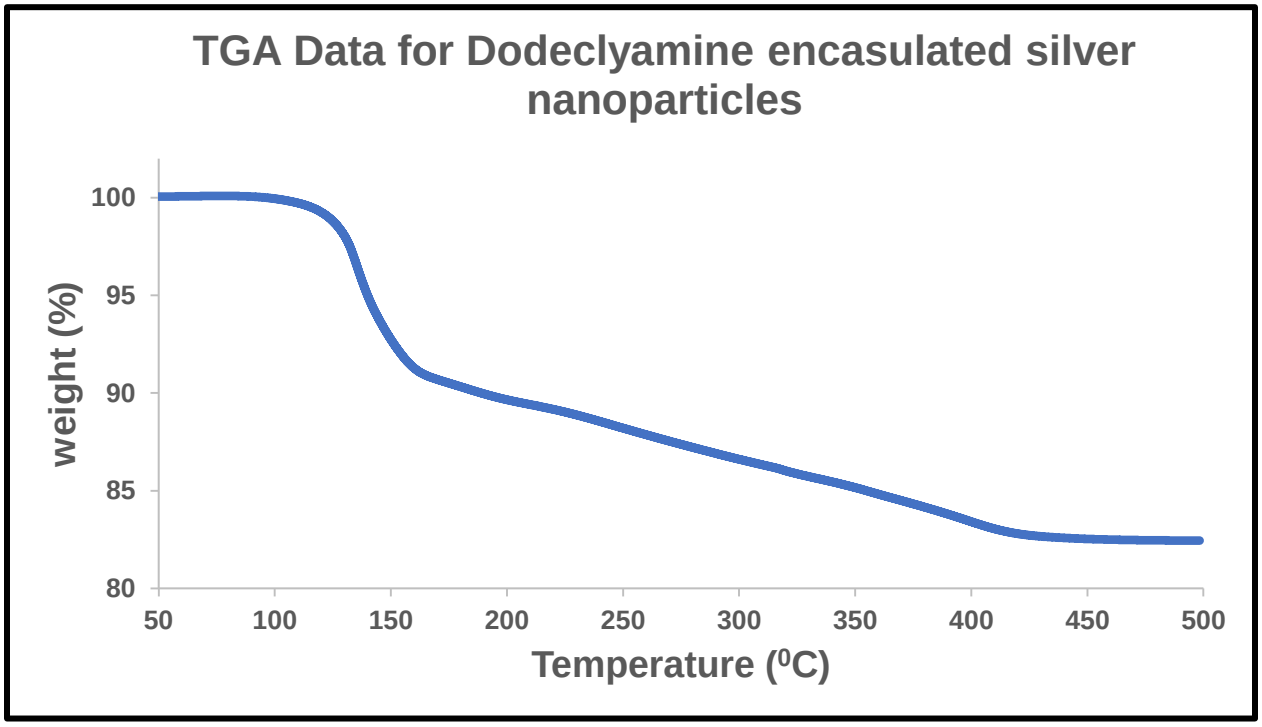

Fig 5.5: TGA data for dodecyl amine encapsulated silver nanoparticles showing the presence of residual ligands during sintering.

During the sintering process, in case of the faster ramp rates, the ligands evaporate from the interior of the system very rapidly. Thus, it allows no time for any surface diffusion between particles and subsequently there is no necking observed in these films. As a result, more of the sintering process occurs with less stabilizers around. This results in more rapid coalescence, leading to the denser films as observed in Fig. 5.6. While on the other hand, in case of the slow ramp rates, most of the ligands are still present in the system during sintering. Thus, the ligands act as solvents to promote surface diffusion of atoms between nanoparticles. This results in the characteristic neck formation between sintered nanoparticles that is observed throughout the film (Fig. 5.3 (a)). The following figure (Fig. 5.6) helps explain the evolution of densification nanoparticle pictorially.

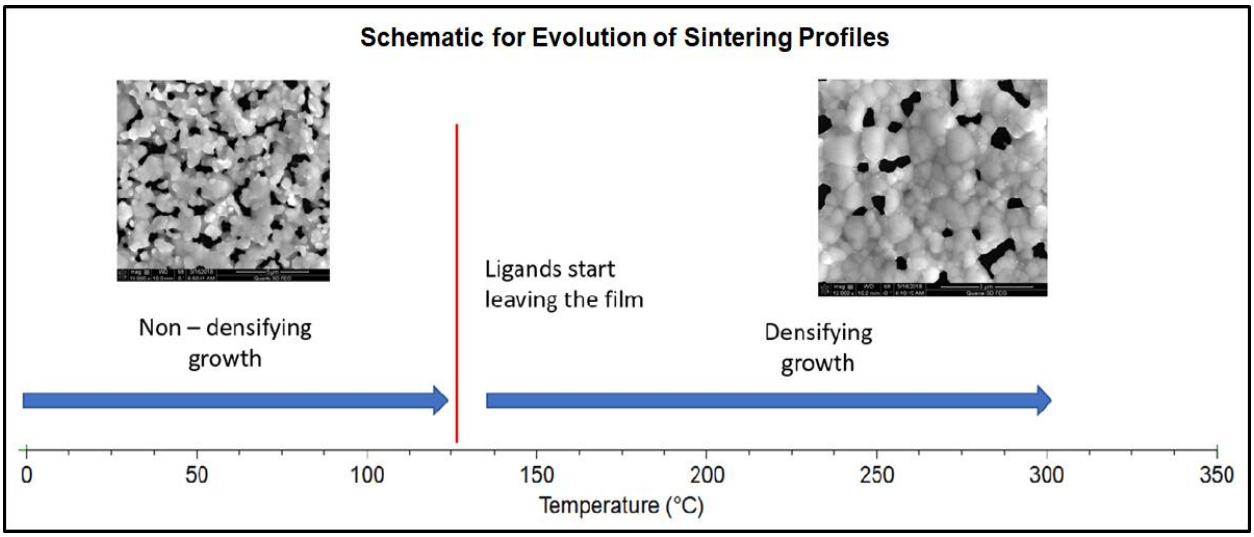

Fig 5.6: Schematic showing the evolution of densification of nanoparticle in a sintered film.

As can be seen from the schematic above, for the films moving through the temperature timeline slowly, most of the sintering happens in the presence of ligands. As a result, surface diffusion dominates the growth mechanism and we see the characteristic neck formation throughout the film. While on the other hand, for samples that ramp through the temperature profile quickly, most of the sintering happens in the absence of ligands. This is because as the system gets to higher temperatures, most of the ligands have already left the system (as shown in Figure 5.5). Thus, the particles can no longer undergo surface diffusion and lattice diffusion becomes the dominant mechanism for growth. This leads to the denser films as shown in Figure 5.3 (b).

5.3. Summary

In this chapter, an explanation was provided to help understand the varying morphologies of the nanoparticle films that were sintered at different temperature ramp rates. The two competing natures of nanoparticle growth were discussed and a chronological order was developed to understand the evolution of the films at different stages in the sintering process. Finally, the influence of these resulting morphologies on the mechanical properties were discussed. This understanding can now be used towards altering sintering conditions to provide stronger nanoparticle bonds for solder replacement application.

Chapter 6. Conclusion and Future Work

This thesis has discussed several different material systems for electronic packaging applications as well as the use of different printing technologies to achieve them. In this final chapter, I will review the important takeaways from each of the previous chapters and provide an outlook for the potential future work that is necessary to enhance our understanding of the subject.

6.1. Review In this work, we studied the nature of bonding in various copper particle systems. In each of the systems that we presented here, we investigated the electrical and mechanical properties of the deposited films and evaluated them as potential replacements for eutectic solders in electronic packaging applications. All the systems were carefully chosen keeping in mind the ease of formulating inks for the additive manufacturing processes that were used (i.e. inkjet printing and stencil printing)

The first material system that was discussed was the commercial copper nanoparticle ink provided by Pvnanocell. This system was chosen due to its high mass loading and ease of deposition using conventional inkjet printing techniques. Although this ink demonstrated high electrical conductivity and mechanical strengths, the processing temperatures were too high for the current thermal budgets imposed on integrated circuit manufacturing. As a result, this ink was determined to be not viable for electronic packaging applications.

The next system that was explored were the copper sol-gels. Sol-gels, in general, are easy to formulate and remain stable for a long time. This is critical for a copper system which susceptible to oxidation upon exposure to air. Although these inks demonstrated a pathway for achieving conductive films below 200 ^{0}C, the porosity in the films led to weak mechanical strengths of the bonded structures. These limitations prevented this system from being ideal candidates for solder replacement applications in integrated circuits.

The PVP-CTAB copper nanoparticle inks were the next topic of discussion. These in-house inks provided air-stable copper nanoparticles with an ability to form conductive films at low temperatures. Furthermore, given our understanding of nanoparticles in general, they also provided an easier way to formulate inks for the various printing technologies used here. However, the aggregation of the nanoparticles in the ink due to weak binding of the ligands led to poor contact between the bonding surfaces resulting in weak bond strengths of the interconnects.

Finally, the last chapter was focused on understanding the influence of the various processing parameters on the final film morphologies. This was important as most of the previous systems had failed due to poor mechanical contact between the bond dies and the rough films. Specifically, this chapter discussed the influence of the temperature rates in the sintering profile on the morphology of the films. It was also shown that different morphologies result in different mechanical strengths. Thus, indicating that temperature ramp rate can be used as knob to alter the mechanical properties of sintered nanoparticle films for electronic packaging applications.

6.2. Future Work

Although this work has demonstrated several metal synthesis routes that could potentially be used to replace eutectic solders in electronic packaging applications, there has not been one system that has fulfilled all the requirements. Some of them (PVP-CTAB based nanoparticles and Sol-gels) have provided good electrical conductivity at low temperatures while others (Pvnanocell ink) have illustrated high mechanical strengths. As a result, further exploration is required to find a particle system that can provide good conductivity and mechanical strengths while still maintaining processing temperatures within the current thermal budgets for integrated circuit manufacturing. Furthermore, a deeper understanding of the influence of the fluid properties of the inks and print parameters in the jetting waveform on the jettability of inks is required to formulate printable inks for the various printing technologies discussed in this work.

Finally, the last chapter of this thesis discussed the effect of the temperature ramp rate on the morphology and mechanical strengths of the sintered nanoparticle films. The initial studies provided some understanding on the nature of growth of nanoparticle. However, the influence of other factors like the final anneal temperature, time, ligand system and sintering ambient were not investigated. A detailed understanding of the evolution of nanoparticle growth and their effect on other bulk properties like electrical conductivity (in addition to morphology and mechanical strength) can aid in the development of a system that can be used in electronic packaging applications.

References

[1] R. Tummala, E. J. Rymaszewski, and A. G. Klopfenstein, *Microelectronics Packaging Handbook: Semiconductor Packaging*, 2nd ed. Springer US, 1997.

[2] K. B. Unchwaniwala and M. F. Caggiano, “Electrical analysis of IC packaging with emphasis on different ball grid array packages,” in *2001 Proceedings. 51st Electronic Components and Technology Conference (Cat. No.01CH37220)*, 2001, pp. 1496–1501.

[3] D. T. Siewert, “Properties of Lead-Free Solders,” p. 77.

[4] G. E. Moore, “Cramming more components onto integrated circuits, Reprinted from Electronics, volume 38, number 8, April 19, 1965, pp.114 ff.,” *IEEE Solid-State Circuits Society Newsletter*, vol. 11, no. 3, pp. 33–35, Sep. 2006.

[5] B. Derby, “Inkjet Printing of Functional and Structural Materials: Fluid Property Requirements, Feature Stability, and Resolution,” *Annual Review of Materials Research*, vol. 40, no. 1, pp. 395–414, 2010.

[6] H. C. Nallan, J. A. Sadie, R. Kitsomboonloha, S. K. Volkman, and V. Subramanian, “Systematic Design of Jettable Nanoparticle-Based Inkjet Inks: Rheology, Acoustics, and Jettability,” *Langmuir*, vol. 30, no. 44, pp. 13470–13477, Nov. 2014.

[7] Y. Li, Y. Wu, and B. S. Ong, “Facile Synthesis of Silver Nanoparticles Useful for Fabrication of High-Conductivity Elements for Printed Electronics,” *J. Am. Chem. Soc.*, vol. 127, no. 10, pp. 3266–3267, Mar. 2005.

[8] P. Buffat and J.-P. Borel, “Size effect on the melting temperature of gold particles,” *Phys. Rev. A*, vol. 13, no. 6, pp. 2287–2298, Jun. 1976.

[9] J. R. Greer and R. A. Street, “Thermal cure effects on electrical performance of nanoparticle silver inks,” *Acta Materialia*, vol. 55, no. 18, pp. 6345–6349, Oct. 2007.

[10] J. H. Park *et al.*, “Low-Temperature, High-Performance Solution-Processed Thin-Film Transistors with Peroxo-Zirconium Oxide Dielectric,” *ACS Appl. Mater. Interfaces*, vol. 5, no. 2, pp. 410–417, Jan. 2013.

[11] “Sicrys IC50TM-8,” *PvNanoCell*. [Online]. Available: http://www.pvnanocell.com/sicrys-ic50tmndash8.html. [Accessed: 22-Jun-2018].

[12] “The roles of wettability and surface tension in droplet formation during inkjet printing | Scientific Reports.” [Online]. Available: https://www.nature.com/articles/s41598-017-12189-7. [Accessed: 22-Jun-2018].

[13] A. G.-S. Germany, “ALLRESIST GmbH - Strausberg, Germany,” *Allresist EN*, 01-Mar-2013. .

[14] D. T. Siewert, “Properties of Lead-Free Solders,” p. 77.

[15] “Sols, Gels, and Organic Chemistry,” in *Ceramic Materials*, Springer, New York, NY, 2007, pp. 400–411.

[16] A. Angel, “XXXVIII.—Cuprous formate,” *J. Chem. Soc., Trans.*, vol. 89, no. 0, pp. 345–350, Jan. 1906.

[17] D.-H. Shin *et al.*, “A Self-Reducible and Alcohol-Soluble Copper-Based Metal-Organic Decomposition Ink for Printed Electronics,” *ACS Appl. Mater. Interfaces*, vol. 6, no. 5, pp. 3312–3319, Mar. 2014.

[18] A. A. Athawale, P. P. Katre, M. Kumar, and M. B. Majumdar, “Synthesis of CTAB-IPA reduced copper nanoparticles,” *Materials Chemistry and Physics*, vol. 91, no. 2, pp. 507–512, Jun. 2005.
[19] Y. Wu, Y. Li, and B. S. Ong, “Printed Silver Ohmic Contacts for High-Mobility Organic Thin-Film Transistors,” *J. Am. Chem. Soc.*, vol. 128, no. 13, pp. 4202–4203, Apr. 2006.
[20] M. N. Rahaman, *Sintering of Ceramics*. CRC Press, 2007.
[21] J. Choe, J. N. Calat, and G.-Q. Lu, “Constrained-film sintering of a gold circuit paste,” *Journal of Materials Research*, vol. 10, no. 4, pp. 986–994, Apr. 1995.
[22] S. K. Volkman, S. Yin, T. Bakhishev, K. Puntambekar, V. Subramanian, and M. F. Toney, “Mechanistic Studies on Sintering of Silver Nanoparticles,” *Chem. Mater.*, vol. 23, no. 20, pp. 4634–4640, Oct. 2011.
[23] J. A. Sadie and V. Subramanian, “Three-Dimensional Inkjet-Printed Interconnects using Functional Metallic Nanoparticle Inks,” *Advanced Functional Materials*, vol. 24, no. 43, pp. 6834–6842.